Quaternary Science Reviews 369 (2025) 109586

Contents lists available at ScienceDirect

Quaternary Science Reviews

journal homepage: www.elsevier.com/locate/quascirev

Stable isotopes constrain the genesis of Thar Desert gypsum playas and reveal Holocene paleoenvironmental variability in Northwest India

Alena Giesche [a,1,*], Cameron A. Petrie [b,**], Yama Dixit [c], Fernando Gázquez [d,e], Thomas Bauska [f], Alexandra V. Turchyn [a], Harold J. Bradbury [g], Rachel K. Smedley [h], Vikas K. Singh [i], Ravindra N. Singh [i], David A. Hodell [a]

[a] Department of Earth Sciences, University of Cambridge, Cambridge, United Kingdom
[b] Department of Archaeology, University of Cambridge, Cambridge, United Kingdom
[c] Centre for Atmospheric Sciences, Indian Institute of Technology Delhi, New Delhi, India
[d] Department of Biology and Geology, Universidad de Almería, Almería, Spain
[e] Andalusian Centre for Global Change - Hermelindo Castro (ENGLOBA), Universidad de Almería, Almería, Spain
[f] British Antarctic Survey, Cambridge, United Kingdom
[g] Department of Earth, Ocean and Atmospheric Sciences, University of British Columbia, Vancouver, Canada
[h] Department of Geography & Planning, University of Liverpool, Liverpool, United Kingdom
[i] Department of Ancient Indian History Culture & Archaeology, Banaras Hindu University, Varanasi, India

ARTICLE INFO

Handling Editor: Mira Matthews

Keywords:
Gypsum hydration water
Playa lake
Paleoclimate
Isotope geochemistry
Indus

ABSTRACT

Numerous evaporative saline playa lakes exist within the Thar Desert in Northwest India. Some are active seasonally, whereas others are dry and preserve up to several meters of sedimentary deposits. These deposits feature a variety of evaporite minerals, including the hydrated mineral gypsum ($CaSO_4{\cdot}2H_2O$). The isotopic composition of gypsum hydration water preserves the $\delta^{18}O$ and δD of paleolake water at the time of gypsum formation. This provides a way to understand the hydrologic balance in a part of the world where it is typically very difficult to obtain any paleoclimate records. We present paleohydrological records from two dry playas (Karsandi, Khajuwala) and one active playa (Lunkaransar) in the Thar Desert using the oxygen and hydrogen isotopic composition of gypsum hydration water. We present a theoretical model to explain differences in how the gypsum records water isotopic composition from perennial playas (consistent paleoclimate recorders) as opposed to seasonally fed or ephemeral playas (that reflect evaporated meteoric water inconsistently). Results suggest that enhanced direct precipitation, with associated higher groundwater and possibly fluvial sources, maintained active playa lake basins in the central Thar Desert for the Early through Middle Holocene. We also examine $\delta^{34}S_{SO4}$, $\delta^{18}O_{SO4}$, and $^{87}Sr/^{86}Sr$ of the gypsum sulfate to explore the source and evolution of solutes in the Thar Desert playas. Results indicate that seasalt aerosols likely accumulated in aeolian sands during glacial dry periods and concentrated in playa deposits once a threshold level of moisture was reached in the Early Holocene. By the Late Holocene, after c. 4.4 ka BP, these water sources diminished and some playas were again covered by aeolian deposits. The Thar Desert gypsum deposits provide valuable insight into local moisture balance during a time period that featured important cultural transformation in the surrounding region, including the South Asian Neolithic agricultural societies around 8 ka BP, the full span of the Indus Civilization (5.3–3.3 ka BP), and periods of human occupation after 3 ka BP.

1. Introduction

The Thar Desert, an area covering approximately 200,000 km^2 with annual rainfall of 100–500 mm, stretches across western India (almost the entire state of Rajasthan) and eastern Pakistan. As the most densely populated desert in the world with a population of more than 16 million

* Corresponding author.
** Corresponding author.
E-mail addresses: agiesche@usgs.gov (A. Giesche), cap59@cam.ac.uk (C.A. Petrie).
[1] Present address: Alaska Science Center, US Geological Survey, Anchorage, Alaska 99508, USA.

https://doi.org/10.1016/j.quascirev.2025.109586
Received 12 June 2025; Received in revised form 20 August 2025; Accepted 21 August 2025
Available online 1 September 2025

people today, the Thar Desert presents a unique and rich cultural history flourishing in an extreme environment. Adaptations to drought, heat, and general water scarcity are essential, and have led to innovative architecture, the use of unique endemic plants, and distinctive nomadic lifestyles (Arora et al., 2010; Baghel et al., 2024). The Thar Desert is surrounded by Bronze Age archaeological sites of the Indus Civilization.

The Thar Desert features expanses of gypsum and calcrete deposits, which reveal a dynamic past climate. Although such continuous sedimentary deposits are diagnostic of regions where evaporation exceeds inflow (i.e., arid regions), these deposits can only form when the necessary solutes are available and when the moisture supply is sufficient to dissolve and accumulate the solutes in low-lying areas. Lacustrine gypsum may precipitate in so-called saline playas, which have a negative water budget for most of the year (Rosen, 1994), as well as >5000 ppm of dissolved solutes (Hardie et al., 1978). Solute precipitation begins with the least soluble minerals (e.g., calcite and dolomite) and then progresses to gypsum and halite on the more soluble end of the spectrum (Schreiber and El Tabakh, 2000).

The Geological Survey of India (GSI) has surveyed the vast quantities of gypsum in Rajasthan, which contains >1000 million tons of gypsum reserves and provides over 90 % of the gypsum mined in India, mainly used for cement production, among other industrial uses (Shrivastava et al., 2011). Gypsum is found across playas of the Thar desert, along with other evaporites such as halite and calcite (Roy and Smykatz-Kloss, 2007). Deeper (250–1000 m) deposits of ancient evaporites stem from the Hanseran Evaporite Group (Shrivastava et al., 2011). Mapping gypsum deposits from available GSI maps indicates accumulation in low-lying depressions, valleys, and paleochannels, often following a NE-SW trend that suggests a tectonic or paleochannel control on drainage (Fig. 1) (Sundaram and Rakshit, 1994).

Playa lake systems are attractive to study because of their location in sensitive ecosystems where small changes in rainfall have a great impact. Playa lakes in the Thar Desert have received attention for their paleoclimatic and archaeological significance (Singh et al., 1972; Kajale and Deotare, 1997; Prasad and Enzel, 2006; Madella and Fuller, 2006; Roy and Singhvi, 2016; Deotare et al., 2022), but the gypsum deposits specifically have not been extensively researched. Two studies laid out pioneering groundwork describing the distribution, morphology, and

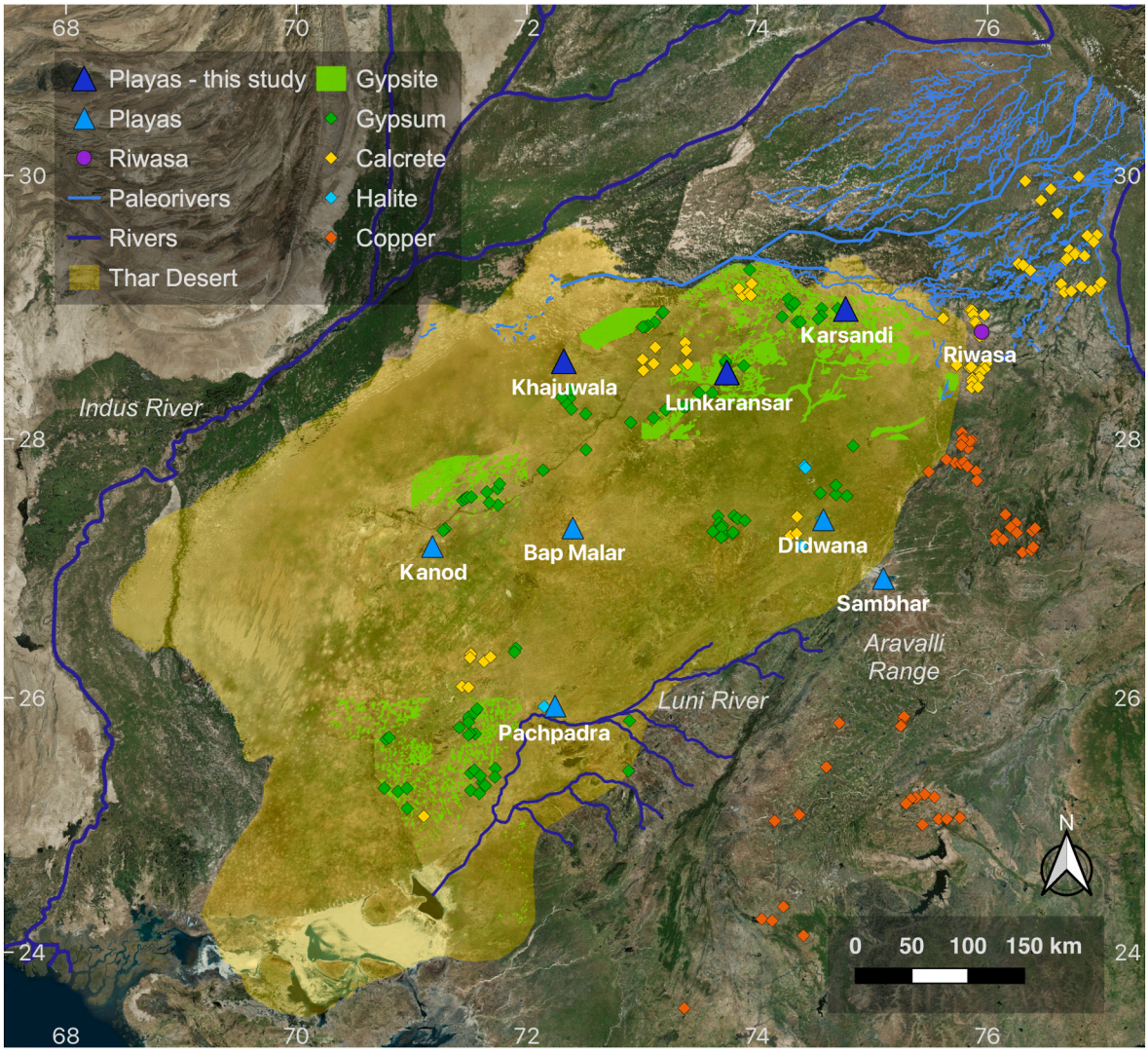

Fig. 1. Present-day river channels (dark blue) and paleoriver channels (light blue) in the interfluve region (Orengo and Petrie, 2017) surround the Thar Desert (yellow shading). Surficial gypsite interdunal valley deposits (green) and gypsum, calcrete, halite, and copper mines (green, yellow, turquoise, and orange diamonds, respectively) were reconstructed from available Geological Survey of India (GSI) maps. Unmapped areas include the western Thar Desert in Pakistan, also known as the Cholistan Desert (considering that many local ancient structures feature gypsum block walls, it is very likely that significant gypsum deposits extend into this area). The three gypsum-rich playa lakes (dark blue triangles) sampled as part of this study include Khajuwala, Lunkaransar, and Karsandi, the water sampling location at Riwasa is shown as a purple circle, and other playas are shown with smaller light blue triangles.

potential climatic implications of gypsum deposits in the Thar Desert, highlighting the difference between lacustrine bedded gypsum and pedogenetic crusts with massive, powdery, or nodular gypsum (Sundaram and Rakshit, 1994; Rakshit and Sundaram, 1998). Dixit et al. (2018) provided the first detailed paleoclimatic interpretation of the Karsandi gypsum deposit in the northern Thar Desert.

The source of solutes to such an extensive region of the Thar Desert, particularly sulfate for gypsum formation, remains an open question, because saline lakes require not only evaporation to exceed inflow but also a perennial source of inflow to maintain their salinity (Eugster, 1980). Solutes are most commonly transported by rivers or streams, storm runoff, or perennial springs, and generally involve a component of bedrock or surficial sediment weathering within the catchment (Eugster, 1980). Paleochannels underlying the playas, even if inactive on the surface, might route groundwater containing solutes to actively recharge the lake. The surficial sediments of the Thar Desert feature a vast supply of sand deposits, which contain marine-derived aeolian material (notably, foraminifera are found in Thar Desert sand up to 800 km north of the Arabian Sea) (Goudie and Sperling, 1977). Finally, the underlying geology needs to be considered: ancient marine evaporites underlie much of the Thar Desert region (Wadhawan and Kumar, 1996; Banerjee et al., 2012; Cozzi et al., 2012), and consequently, deep saline aquifers or brine springs could be another source of solutes. Source interpretations can be derived from the analysis of the sulfur and oxygen isotopic composition of sulfate (SO_4^{2-}) in gypsum (e.g., Sun et al., 2018) as well as measurement of $^{87}Sr/^{86}Sr$ that readily substitutes for the calcium component (e.g., Denison et al., 1998).

Gypsum is also a uniquely useful paleoenvironmental recorder. Gypsum ($CaSO_4{\cdot}2H_2O$), a hydrated evaporite mineral, consists of 20.9 % water by weight. This structurally bonded crystallization water, also known as gypsum hydration water (GHW), can remain unaffected by post-depositional processes such as re-crystallization or isotope exchange via water diffusion (Gázquez and Hodell, 2022) and thereby reflects the oxygen and hydrogen isotopic composition of the water in which it was formed (Sofer, 1978; Khademi et al., 1997; Hodell et al., 2012). By using the oxygen and hydrogen isotope fractionation factors between GHW and its parent water (which are largely insensitive to temperature and salinity) (Gázquez et al., 2017; Liu et al., 2019), the isotopic composition of the parent solution can be calculated. Thereby, changes in oxygen and hydrogen isotopic composition of evaporated waters can be reconstructed from gypsum deposits in saline lakes. Furthermore, d-excess, a parameter derived from the relationship between $\delta^{18}O$ and δD, is driven by relative humidity conditions as well as temperature (Gázquez et al., 2018), while ^{17}O-excess is generally considered to be a temperature-independent relative humidity indicator (Luz and Barkan, 2010). These measurements provide an insight into the evaporation history of the playa lake through time, allowing us to infer changes in local hydrology, and by extension regional – and even global – climate.

This paper presents three Holocene gypsum records from playa lakes spanning a rainfall gradient in the Thar Desert (Supplemental Fig. 1). In the west-central region, Khajuwala receives 200 mm of annual precipitation and has a relative humidity of 30 % (winter) to 50 % (summer) at present. Lunkaransar in the north-central desert has 260 mm of annual rainfall and 35–55 % humidity, while Karsandi on the north-eastern margin has the highest rainfall of 320 mm per year and average relative humidity ranging 40–55 %. More than 85 % of rainfall at these study sites occurs in the summer (May through October), arriving via the Indian Summer Monsoon and increasing towards the east. Winter rainfall is mainly linked to Western Disturbances (WDs) (Midhuna et al., 2020) carried by westerlies, and is highest in the northwestern part of the Thar Desert. We examine gypsum from these three playa lakes to study the prevailing environmental conditions during deposition, with implications for interpretation of gypsum sequences and the use of gypsum hydration water as a paleoclimate proxy. We also discuss the possible source of solutes for gypsum formation in the Thar Desert, using strontium isotopes and the sulfur and oxygen isotopic composition of sulfate in gypsum. Finally, we consider the archaeological implications of Holocene water availability in the Thar Desert.

2. Materials and methods

2.1. Field

Sediment sections from the three Thar Desert playa lake sites were described and sampled between 2010 and 2019 (Fig. 2).

Khajuwala (28° 35′ 46.932″ N, 72° 19′ 18.084″ E) was identified based on its location as an active gypsum mine and was visited in 2017/2019 with permission of India's Border Security Force. According to the local miners, the gypsum deposits extend ~0.24 km^2, and the deepest sections are 3 m. This would put the maximum gypsum volume at 720,000 m^3, or 2.3 million tons of gypsum. Quaternary flood plain deposits and aeolian sand comprise the surrounding surficial geology. Khajuwala samples were collected at 2-cm resolution from a 3-m deep section exposed by mining, along with three luminescence samples. The sequence can be divided into eight gypsiferous units, with gray and then yellow sand layers below the gypsum and a variably-thick yellow-brown sand layer at the surface (Fig. 2) (see the **Supplemental Materials** for a more detailed description of each unit's characteristics, including mineralogy and identified gastropods and ostracods).

Lunkaransar (28° 28′ 1.96″ N, 73° 42′ 7.99″ E) was sampled in February 2019. The playa is actively used for selenite mining (selenite is a variety of gypsum), and the surrounding surficial geology comprises Quaternary fluvio-lacustrine and aeolian sediments, with gypsite and calcrete pockets in the interdunal valleys. Prior investigation showed that the lake basin is underlain by calcareous deposits, and a >1-m thick sequence of low-permeability clay deposits at the base acts to retain water (Singh et al., 1972). Lunkaransar falls between a set of tectonic lineaments that control the drainage system (Wadhawan and Kumar, 1996), and tectonically-driven stream segmentation has been suggested as the formation mechanism for the depression of this playa lake (Roy, 1999). A 1.36-m-deep exposed trench was cleaned and sampled at 2-cm intervals. Its sediments are wet and partially submerged even during the dry season, which limited the sampling depth. The top 32 cm consist of overburden material (from trench excavation before our sampling). The remaining 104-cm sequence consisted of five units, all containing some form of gypsum crystals except for Unit II (Fig. 2) (see the **Supplemental Materials** for a detailed description of each unit's characteristics).

Karsandi (28° 59′ 29.6″ N, 74° 45′ 53.8″ E) was first identified by Saini et al. (2005). Karsandi lies 21 km south of a paleotributary of the now seasonal Ghaggar-Hakra river (Fig. 1), which was supplied with monsoonal rainfall and water originating in both the Aravalli and Himalayan mountain chains (Orengo and Petrie, 2017). Besides collecting and channeling groundwater and moisture today, the presence of paleochannels raises the question of whether active streams or rivers could have fed Karsandi via surface overflow or flooding during rainier periods in the past. Karsandi's gypsum sequence was sampled at 2-cm resolution in 2010 and was revisited for two luminescence dates and additional sampling in 2014 (Dixit, 2013; Dixit et al., 2018). Its 2.2-m sequence consists of eight gypsum-rich units (Saini et al., 2005; Dixit et al., 2018) underlain by yellow-brown sand, and overlain by 47 cm of sand at the surface. The published $\delta^{18}O$ and δD gypsum dataset and age model (Dixit et al., 2018) was augmented in this study by adding $\delta^{17}O$, $\delta^{34}S_{SO4}$, $^{87}Sr/^{86}Sr$, and $\delta^{18}O_{SO4}$ data.

In addition, we sampled Thar Desert water from 19 sites (wells,

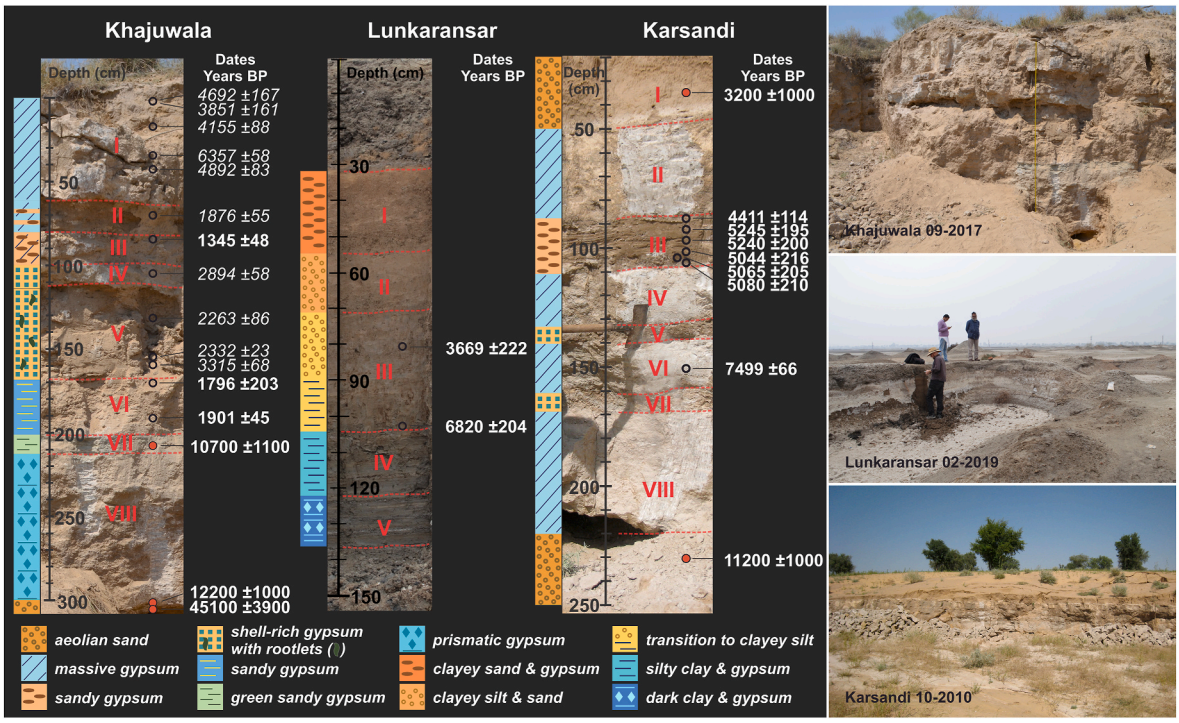

Fig. 2. Sediment lithologs and chronology for the three playa sequences (left) and landscape overview photos from the three playas (right), with AMS dates (open black circles) and luminescence dates (orange circles with black outlines). *Italicized* dates for Khajuwala fall out of sequence and were not used for the chronology). Roman numerals signify distinct units within each of the stratigraphic columns.

ponds, lakes, reservoirs) during the 2017/2019 fieldwork seasons and combined these with six Riwasa well water measurements from 2010 (Dixit, 2013) in order to establish a local evaporative line (LEL) baseline (Supplemental Fig. 2). We additionally conducted a 36-h pan evaporation experiment near Khajuwala (28° 41′ 22.092″ N, 72° 35′ 13.848″ E) in February 2019 to investigate the desert's diurnal evaporation characteristics as an analogue for summer vs. winter conditions (these results are not further discussed here, but see the **Supplemental Materials**, including Supplemental Tables 1–3 for more details).

2.2. Laboratory analyses

2.2.1. Chronology

A total of 20 Accelerator Mass Spectrometry (AMS) dates were run on the Khajuwala sequence, based mainly on *Zootecus insularis* shells as well as plant remains (Supplemental Table 4). Lunkaransar's samples yielded a piece of charcoal and a shell fragment for AMS dating (Supplemental Table 5). AMS and luminescence dates for Karsandi are described in Dixit et al. (2018). Samples for AMS radiocarbon dating were picked out of the wet-sieved >300 μm size fractions. Five samples were measured with conventional AMS at the University of Oxford, and all other AMS dates were analyzed at the University of Bern using a MICADAS system specialized for small samples sizes. Luminescence dating of three samples from Khajuwala (KF2, KF6 and KF7) was performed at the University of Liverpool using density-separated K-feldspar grains (90–125 μm) to determine the paleodose, which was divided by the environmental dose-rate derived using high-resolution gamma spectrometry to determine ages. The **Supplemental Materials** contain additional AMS and luminescence method details.

2.2.2. Mineralogy

The mineralogy of the playa lake deposits, as well as the overlying and underlying aeolian sands, were investigated with X-Ray Diffraction (XRD) and Scanning Electron Microscope (SEM) instruments (see **Supplemental Materials** for details of the methods). The assessed XRD samples included Khajuwala (n = 13) and Lunkaransar (n = 8). Karsandi was not measured due to lack of sample material.

2.2.3. Stable isotope ratios of gypsum hydration water

Two methods were used to measure gypsum hydration water isotope ratios: the "off-line" method for large sample sizes (>150 mg) that was used for the majority of samples, and the "on-line" method for a few samples where we had limited amounts. The main difference in results is that the on-line method does not produce ^{17}O results, due to the different instrumentation used for this set-up, but all other results are comparable (see **Supplemental Materials** for more details). All samples were analyzed at the Godwin Laboratory at the University of Cambridge.

The off-line gypsum hydration water extraction method follows Gázquez et al. (2015). Gypsum was present between 47 and 223 cm depth at Karsandi (82 total samples, including seven depths run in duplicate or triplicate), Khajuwala gypsum spanned 0.5–298 cm (280 total samples, with duplicates or triplicates run for more than half of the depths), and Lunkaransar's section featured gypsum at 30–56 cm and 92–136 cm depth (40 total samples with five depths run in duplicate or triplicate). The water oxygen and hydrogen isotopes (^{16}O, ^{17}O, ^{18}O, ^{1}H, ^{2}H) were then measured using Cavity Ring-Down Spectroscopy (CRDS) with a Picarro L2140i, equipped with a A0211 high-precision vaporizer. The results were calibrated using four internal water standards (JRW, BOTTY, SPIT, and ENR), which were calibrated against the international water standards Vienna Standard Mean Ocean Water (VSMOW) and Standard Light Antarctica Precipitation (SLAP), and are thus reported relative to VSMOW-SLAP. A NEWGYP in-house gypsum standard was extracted with each set of five gypsum samples to assess reproducibility, showing ± 1σ analytical precision of 0.2 ‰ for $\delta^{18}O$, 0.1 ‰ for $\delta^{17}O$, and 0.8 ‰ for δD

(Supplemental Table 6). The precision was 12 per meg for ^{17}O-excess and 1 ‰ for d-excess.

For n = 15 size-limited gypsum samples (<150 mg) from Lunkaransar, the alternative on-line method was applied using the combined NETZSCH TGA and Picarro L2130i differential thermal isotope analysis (DTIA) approach (Bauska et al., 2018) (see **Supplemental Materials** for more details), which only delivers ^{16}O, ^{18}O, ^{1}H, and ^{2}H results (not ^{17}O). A set of internal gypsum standards (DEVAUX, GEODA, SALINA, and UALGYP) were each run three times before the samples to provide a gypsum-based calibration for the NETZCH-Picarro procedure. Three NEWGYP standards were included for the NETZSCH extraction of 15 samples, yielding ± 1σ analytical precision of 0.04 ‰ for $\delta^{18}O$ and 1.0 ‰ for δD (Supplemental Table 6).

The raw isotopic composition of the gypsum hydration water is corrected to reflect the true "parent water" isotopic composition by using the known gypsum formation fractionation (α) factors: 1.003464 for $\delta^{18}O$, 0.9807 for δD, and 1.001833 for $\delta^{17}O$ (Gázquez et al., 2017), also supported by theoretical predictions (Liu et al., 2019). These α factors assume a temperature of 25 °C and salinities <30 g/L (realistic for these Thar Desert playas where gypsum is the main precipitate). The α factors are generally unaffected by a temperature range of 10–35 °C, and $\alpha^{18}O$ is unaffected by salinities <150 g/L, whereas αD increases with salinities >30 g/L (Gázquez et al., 2017). Diagenesis or isotopic exchange is unlikely to affect large (>250 μm) gypsum crystals after primary deposition in the playa has occurred (Gázquez and Hodell, 2022), and our samples exceeded this size threshold (e.g., **Supplemental Materials**). We thereby assume that all GHW results discussed in the following sections reflect the parent (playa) water isotopic composition.

2.2.4. Oxygen ($\delta^{18}O_{SO4}$) and sulfur ($\delta^{34}S_{SO4}$) isotopic composition measurements

For the Khajuwala sequence, the $\delta^{34}S_{SO4}$ and $\delta^{18}O_{SO4}$ of the sulfate in the gypsum was measured for 20 depths (4 depths in triplicate for $\delta^{34}S_{SO4}$, and all $\delta^{18}O_{SO4}$ in duplicates). At Lunkaransar, the $\delta^{34}S_{SO4}$ and $\delta^{18}O_{SO4}$ was measured for 28 and 8 depths, respectively (5 triplicates for sulfur, and all samples in duplicate or triplicate for oxygen). The $\delta^{34}S_{SO4}$ and $\delta^{18}O_{SO4}$ was determined for 10 depths throughout the Karsandi sequence, all of which were replicated for $\delta^{34}S_{SO4}$, and 5 depths which were replicated for $\delta^{18}O_{SO4}$.

Gypsum powder (from the gypsum hydration water preparation steps) was re-precipitated as $BaSO_4$ to analyze its $\delta^{34}S_{SO4}$ and $\delta^{18}O_{SO4}$ (see **Supplemental Materials** for additional details). The $\delta^{18}O_{SO4}$ was measured by pyrolysis in a TC/EA coupled to a Delta V Mass Spectrometer in the Godwin Laboratory for Paleoclimate Research, and $\delta^{34}S_{SO4}$ was determined by flash combustion in a Flash EA under excess oxygen coupled to a Delta V Mass Spectrometer by continuous flow, also in the Godwin Laboratory. Samples were bracketed with the NBS-127 barite standard ($\delta^{34}S_{SO4}$ of 20.3 ‰ and $\delta^{18}O_{SO4}$ of 8.6 ‰) to correct for measurement drift. All results are reported with respect to Vienna Canyon Diablo Troilite (V-CDT) for $\delta^{34}S_{SO4}$ (‰) and VSMOW for $\delta^{18}O_{SO4}$ (‰).

2.2.5. Sr isotope measurements

For Khajuwala, the $^{87}Sr/^{86}Sr$ was determined for 11 of the 20 depths previously assessed in the SO_4 analysis. At Lunkaransar, 8 of the 28 depths were assessed, and for Karsandi, the $^{87}Sr/^{86}Sr$ was measured for 9 out of the 10 depths, with 1 replicate.

For Sr isotope measurements, Sr concentrations of the gypsum powder were first assessed by ICP-OES (Agilent 5100). Based on these results, an aliquot containing 300 ng of Sr was dried down and re-dissolved in HNO_3 in preparation for standard column chemistry. Acid- and Milli-Q-water-cleaned columns received Eichrom Sr Specific resin and the Sr fraction was collected in acid-clean Teflon beakers. Sr samples were dried down in nitrate form for analysis on the Thermo Scientific Triton Plus Thermal Ionization Mass Spectrometer (TIMS). Samples were loaded onto outgassed single Rhenium filaments with Ta activator and run alongside five NBS 987 standards per turret to assess the external reproducibility of the isotope ratio measurement. All analyses were conducted at the University of Cambridge (see **Supplemental Materials** for additional details).

3. Results

3.1. Chronology

The previously published Karsandi chronology includes seven AMS radiocarbon dates from terrestrial gastropods and charophytes, accompanied by two luminescence dates (Dixit et al., 2018). These two luminescence dates from the sand above and below the gypsum yielded boundary dates for the emergence of the playa lake (11.2 ± 1 ka BP) until its complete desiccation (3.2 ± 1 ka BP). Several terrestrial gastropods were dated in Unit III (within 4.3 and 5.3 ka BP) along with charophytes from Unit VI (c. 7.5 ka BP); however, no other units contained enough dateable material to provide an acceptable age depth model. Therefore, the ages of transitions between units at Karsandi remain imprecise.

At Khajuwala, luminescence dating places the lower gray aeolian sand (307–312 cm depth) at 45.1 ± 3.9 ka BP (see Supplemental Table 7 for dose rate calculations and Supplemental Fig. 3 for Abanico plots of equivalent dose values). XRD analysis of the sand shows the presence of gypsum among other common minerals (e.g., quartz, calcite, albite, kaolinite, rutile, illite, and chlorapatite) (Supplemental Fig. 4). The immediately overlying yellow aeolian sand (300–305 cm) constrains the beginning of gypsum accumulation to younger than 12.2 ± 1 ka BP (Supplemental Table 4). A luminescence date taken from the gray-green gypsiferous sandy Unit VII (201–211 cm) is dated to 10.7 ± 1.1 ka BP. Thirteen AMS radiocarbon dates on terrestrial gastropods were obtained from Units I-VI (ranging between 1.3 and 6.4 ka BP), but most of them do not correspond to their stratigraphic order and indicate reworking (Fig. 2, Supplemental Table 4). Freshwater aquatic gastropods and brackish water ostracods appear in Unit V, which stands in contrast to the overlying lenticular and cemented massive gypsum with sandy layers and terrestrial gastropods found in Units I-IV (top meter of the sequence). Seven modern AMS radiocarbon dates from plant remains (Units II, IV, and VIII) showed that vegetation, including halophilic algae, had grown deeper into parts of the exposure than we expected. A tentative chronology was adopted (Fig. 2), which accepts all luminescence dates and the three AMS dates that fall in stratigraphic order (ten other AMS dates fall out of order and were not used – see Fig. 2). It follows that the deepest 1 m of laminated gypsum in Units VIII and VII represent a span of c. 2000 years of sequential gypsum deposition during the Early Holocene between 12.2 ± 1 ka and 10.7 ± 1.1 ka BP. In contrast, the top 2 m of the sequence was deposited and subsequently reworked between 1.3 and 1.9 ka BP.

Two AMS radiocarbon dates were obtained from the sequence at Lunkaransar: one from a small fragment of charcoal (113 μg, at 80–82 cm depth) was dated to 3.67 ± 0.2 cal ka BP, and the other from a gastropod (570 μg, at 102–104 cm depth) was 6.82 ± 0.2 cal ka BP (Supplemental Table 5).

3.2. Stable isotope ratios of gypsum hydration water

The maximum and minimum GHW stable isotope values were calculated (Supplemental Table 6) and the mean values were plotted for each playa (Figs. 3–5) after correcting for gypsum hydration water isotope fractionation (Gázquez et al., 2017). Standard deviations (±1σ) were calculated by site for each variable (Supplemental Table 6). For

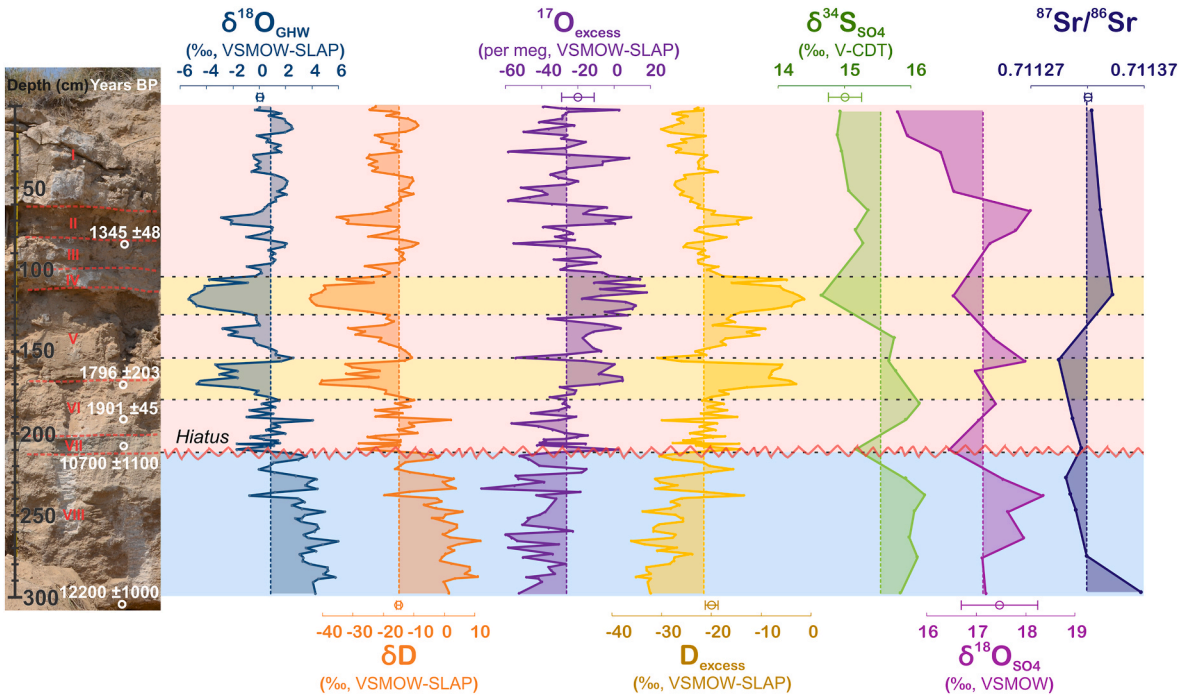

Fig. 3. Khajuwala multiproxy dataset, highlighting Late Holocene (post c. 1.9 ka BP) lenticular gypsum at the top (0–211 cm, red background), which includes two sections of very ^{18}O-depleted GHW and aquatic gastropods (105–127 and 157–173 cm, yellow background), and Early Holocene (c. 12.2–10.7 ka BP) laminated prismatic gypsum at the bottom (211–299 cm, blue background). Selected calibrated ^{14}C and luminescence dates are denoted by white circles with ± 2σ age errors. For each proxy, ± 1σ measurement error bars are shown near the x-axes, and the dotted vertical line represents the mean value for the dataset.

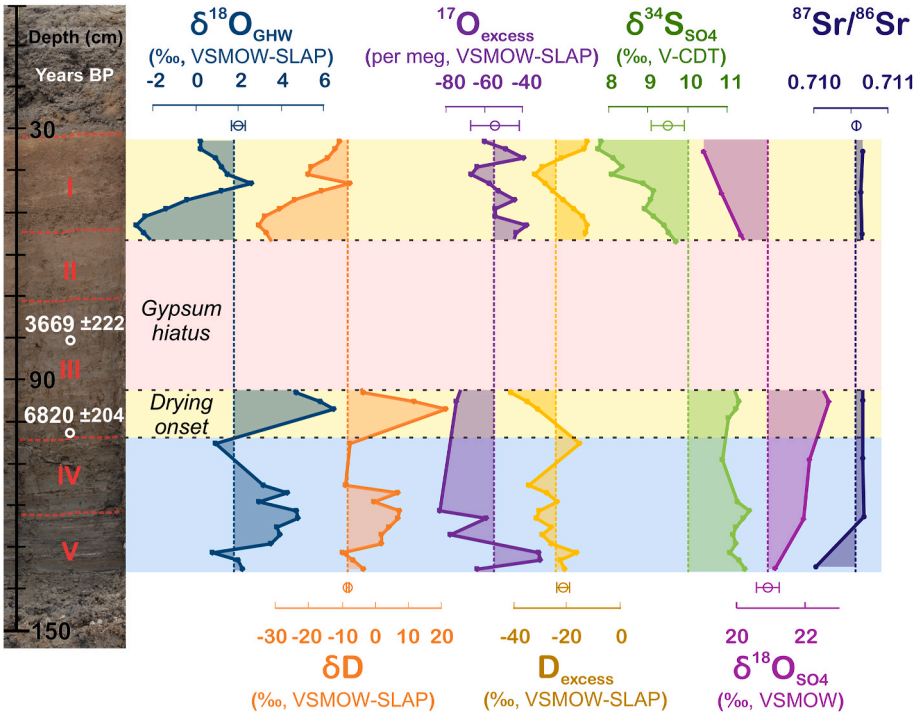

Fig. 4. Lunkaransar multiproxy dataset, highlighting Late Holocene (<4 ka BP) lenticular gypsum at the top (32–56 cm, yellow background), gypsum hiatus (56–93 cm, red background), onset of drying (106 cm, yellow background), and Early-Middle Holocene laminated prismatic gypsum at the bottom (93–136 cm, blue background). Calibrated ^{14}C dates are denoted by white circles with ± 2σ age errors. For each proxy, ± 1σ measurement error bars are shown near the x-axes, and the dotted vertical line represents the mean value for the dataset.

example, for $\delta^{18}O$, standard deviations of the in-house water standard SPIT were between 0.04 and 0.14 ‰ for all sites (measuring Picarro precision), 0.1–0.33 ‰ for the in-house gypsum standard (reflecting Picarro and WASP precision), and 0.47–0.65 ‰ for sample replicates (accounting for sample variability while picking gypsum crystals from the same depth, weighing and crushing the crystals, as well as Picarro

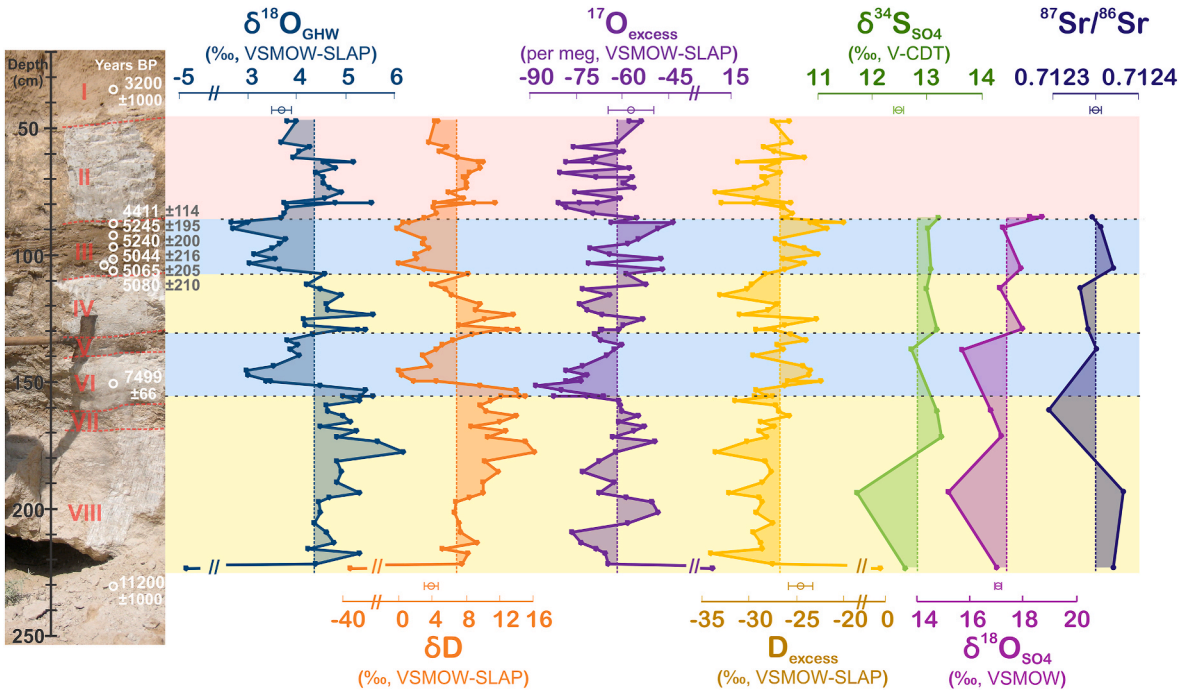

Fig. 5. Karsandi multiproxy dataset showing dates and $\delta^{18}O$, δD, and d-excess reproduced from Dixit et al. (2018) and ^{17}O-excess, $\delta^{34}S_{SO4}$, $\delta^{18}O_{SO4}$, and $^{87}Sr/^{86}Sr$ data from this study. The horizontal panels highlight Late Holocene (c. 4.4–3.2 ka BP) gypsum at the top (46–86 cm, red background), Middle Holocene (c. 5.2–4.4 ka BP) gypsum in the middle (86–115 cm, blue background), and Early-Middle Holocene (c. 11.2–5.2 ka BP) gypsum at the bottom (115–224 cm, blue and yellow backgrounds). Luminescence and calibrated ^{14}C dates are denoted by white circles with ± 2σ age errors. For each proxy, ± 1σ measurement error bars are shown near the x-axes, and the dotted vertical line represents the mean value for the dataset. Double diagonal lines on the x-axis indicate a break in scale.

Table 1
Regression coefficients for slopes in Fig. 6; see full table in Supplement (Supplemental Table 3).

$\delta^{18}O/\delta D$	R^2	Intercept	Slope	SE	T statistic	P value
Thar Desert LEL (n = 26)	0.98	−13.01	5.18	0.17	31.04	6.94E-21
Late Holocene GHW (n = 126)	0.93	−19.86	4.48	0.11	40.01	9.65E-73
Early-Middle Holocene GHW (n = 126)	0.91	−16.62	5.22	0.15	34.48	2.19E-65

and WASP precision).

The d-excess (derived from the $\delta^{18}O/\delta D$ relationship) of the playa samples plot lower than the values given by the modern local evaporation line (Table 1 and Fig. 6) (see the **Supplemental Materials** and Supplemental Figs. 5 and 6 for details on the measurements of modern local evaporation). A shallower slope generally indicates drier atmospheric conditions in the past with more evaporative loss, assuming the source water has not changed (Dansgaard, 1964; Fröhlich et al., 2002). We also split gypsum hydration water samples from all three sites between recent samples (Late Holocene, <4.2 ka BP, includes depths n = 114 from Khajuwala up to 210 cm depth, and n = 12 from Lunkaransar up to 55 cm depth) and older samples (Early and Middle Holocene, 11–4.2 ka BP, includes n = 71 from Karsandi at all depths with gypsum, n = 42 from Khajuwala deeper than 210 cm, and n = 13 from Lunkaransar deeper than 95 cm depth) (Fig. 6, see also **Supplemental Data** and Supplemental Fig. 5). The Late Holocene samples have the shallowest slope ($\delta^{18}O/\delta D$ space) (Table 1), and the $\delta^{18}O$ values are c. 4 ‰ lower than the Early and Middle Holocene samples.

3.3. SO_4 and Sr isotope ratio measurements

Result statistics including maximum and minimum values from gypsum-derived $\delta^{18}O_{SO4}$, $\delta^{34}S_{SO4}$, and $^{87}Sr/^{86}Sr$ are reported in Supplemental Table 8, and means are plotted in Figs. 3–5. Standard deviations (±1σ) are reported from pooled replicates of the samples wherever available. Machine drift was corrected for 27 of the Lunkaransar $\delta^{34}S_{SO4}$ samples using a regression slope from NBS 127 standards run throughout. Blanks for $^{87}Sr/^{86}Sr$ were negligible.

The $\delta^{34}S_{SO4}$ for all playas range from 7.7 to 16.2 ‰, with Lunkaransar at the lower end of the range and Khajuwala at the upper end. The $\delta^{18}O_{SO4}$ ranges from 15.2 to 23.2 ‰, with highest values found at Lunkaransar compared to the other two playas. Covariation between $\delta^{18}O_{SO4}$ and $\delta^{34}S_{SO4}$ is apparent for all playas (Fig. 7a). Both $\delta^{18}O_{SO4}$ and $\delta^{34}S_{SO4}$ trend towards lower values in the upper parts of the Khajuwala and Lunkaransar records (Figs. 3 and 4). The values for $^{87}Sr/^{86}Sr$ range from 0.710600 to 0.712382 (lowest at Lunkaransar, and highest at Karsandi). The $^{87}Sr/^{86}Sr$ of each playa lake is consistent throughout time, with <0.0001 variability within each basin, and c. 0.001 variability between basins.

4. Discussion

4.1. Origin of sand and gypsum in the Thar Desert

Dune activity is an indicator of past climate changes and provides useful context when examining the playa lake records. The origin of

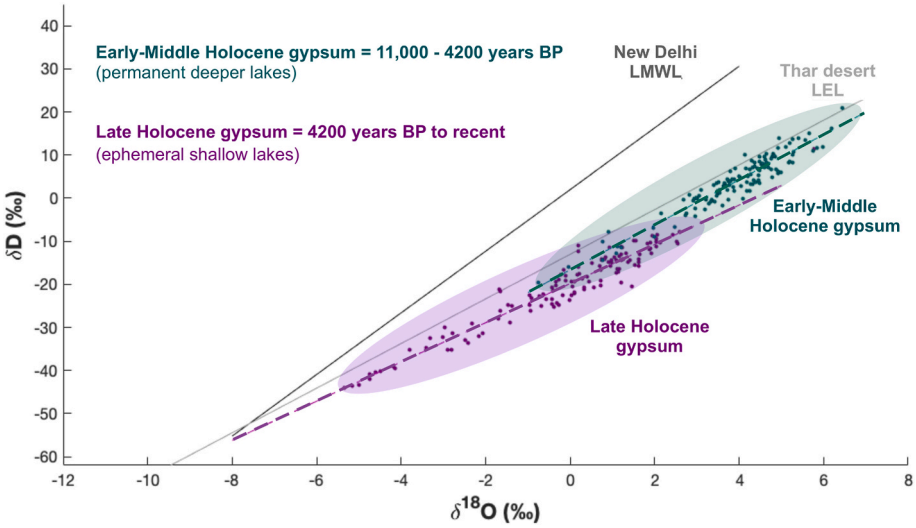

Fig. 6. Regression slope (δD- $\delta^{18}O$) shown in dark gray for the LMWL from New Delhi ($\delta D = 7.15\ \delta^{18}O + 2$) (Pang et al., 2004), the LEL based on Thar Desert groundwater measurements (light gray), Early-Middle Holocene GHW (green), and Late Holocene GHW (purple). Regression slope values are reported in Supplemental Table 3 and ^{17}O-excess and d-excess data from individual playa lakes and their outliers are distinguished in Supplemental Fig. 5.

dune formation in the Thar Desert extends to at least 200 ka BP (Singhvi and Kar, 2004; Singhvi et al., 2010). Despite dry conditions with ample sediment supply during the last glacial maximum, modern dune formation could not properly take place until the Indian Summer Monsoon gained strength c. 14 ka BP (Chawla et al., 1992; Glennie et al., 2002) with increased SW winds contributing to higher sand accumulation (Singhvi and Kar, 2004). Wasson et al. (1983) also describe the dunes of the Thar Desert as a unique kind of desert system that is "formed by the southwest monsoon." Major dune-building episodes occurred during transitions to wetter climates, such as during the Middle Holocene up until c. 7 ka BP (Usman et al., 2024). Thereafter, sustained increases in rainfall and ensuing pedogenesis and vegetation growth eventually shut off this mechanism by c. 6 ka BP in most parts of the Thar Desert (Singhvi and Kar, 2004). Not long after this window of maximum humidity, dune activity recommenced from c. 5 to 3.5 ka BP in parts of the Thar Desert and continued from c. 2 to 1 ka BP, pointing to renewed periods of weakened Indian Summer Monsoon (Thomas et al., 1999; Singhvi and Kar, 2004; Srivastava et al., 2019).

An extensive historical debate exists concerning the source of salts that accumulated in numerous playa lake deposits throughout the Thar Desert. Proposed sources have included intrusion and drying of an inland sea during the Quaternary (Hume, 1867–68, vide Holland and Christie, 1909), accumulation of marine-derived aerosols from the Rann of Kutch (Holland and Christie, 1909; Singh et al., 1972), dissolution of ancient evaporite beds within the basin (Godbole, 1952), weathering of local bedrock and solute transport via fluvial channels (Ramesh et al., 1993; Mathur, 2008), and segmentation of stream channels and aridity leading to the concentration of solutes (Roy, 1999).

Marine-derived solute sources in the Thar Desert have been broadly dismissed in the literature (e.g., Ramesh et al., 1993; Yadav and Sarin, 2009), but the analysis presented here suggests that further examination of this source is warranted. For example, Ramesh et al. (1993) showed that playa water isotopes reflect a meteoric origin rather than ancient marine water and suggested that bedrock weathering contributes solutes. Roy (1999) cited aridity and topographic depressions as the prerequisites for forming saline lakes, but this again does not preclude a marine contribution of salts. Yadav and Sarin (2009) discounted marine salts by comparing marine and lake uranium isotopes in Sambhar playa, but its location on the eastern margin of the desert and influence of nearby Aravalli Mountains bedrock makes this an atypical comparison to the rest of the Thar Desert playas.

A combination of $\delta^{34}S_{SO4}$, $\delta^{18}O_{SO4}$, and $^{87}Sr/^{86}Sr$ signatures of the playa lakes helps constrain the most likely source(s) of solutes to the playas (Fig. 7). Strontium replaces calcium in the lattice of the gypsum crystal, and the $^{87}Sr/^{86}Sr$ signature is maintained as the sediments are transported and when gypsum precipitates; the gypsum should record the $^{87}Sr/^{86}Sr$ of the fluid from which it precipitates. Sulfate in the gypsum, on the other hand, can come from marine sea salt aerosols or weathering of sulfur-bearing minerals in the catchment. The $\delta^{34}S_{SO4}$ is derived from the source of sulfur during weathering, with evaporite minerals and marine sulfate aerosols having higher $\delta^{34}S_{SO4}$ and oxidative weathering of pyrite producing sulfate that has lower $\delta^{34}S_{SO4}$. In contrast, the oxygen atoms in sulfate do not exchange with water, and therefore the $\delta^{18}O_{SO4}$ reflects the pathway of formation the last time the sulfate formed, and where the oxygen atoms might have come from and any fractionation on their incorporation. If the sulfate comes from the weathering of evaporite minerals, then the $\delta^{18}O_{SO4}$ will reflect the $\delta^{18}O$ of the sulfate in the evaporite minerals. However, if the sulfate comes from the oxidative weathering of pyrite, then the $\delta^{18}O_{SO4}$ reflects the pathway of oxidation (Relph et al., 2021). If sulfate is subsequently reduced through microbial sulfate reduction, then the residual sulfate's $\delta^{18}O_{SO4}$ and $\delta^{34}S_{SO4}$ will coevolve due to isotope fractionation associated with microbial sulfate reduction (Antler et al., 2013). Combining the sulfur, oxygen and strontium isotope data presents possible scenarios for the accumulation of Thar Desert solutes.

The $\delta^{18}O_{SO4}$ of the playas are distinct from one another, ranging from 15 to 19 ‰ at Karsandi and Khajuwala, and 19–23 ‰ at Lunkaransar (Fig. 7). These ranges exclude *direct* formation of the gypsum in the playas from a seawater source of sulfate, as marine $\delta^{18}O_{SO4}$ is 8.6 ‰ in the modern ocean and recent past. It has been suggested that there is a 3 ‰ oxygen isotope fractionation during gypsum precipitation, but the $\delta^{18}O_{SO4}$ in the playa gypsum is still more ^{18}O-enriched (Lloyd, 1968; Horibe et al., 1973).

One possible source of solutes to the Thar Desert playas is the bedrock beneath the aeolian deposits. The Hanseran Evaporite Group (HEG) is a 100–650 m-thick late Neoproterozoic to early Cambrian stratum containing cycles of halite, gypsum, and carbonate, which occurs anywhere from 250 to 1100 m below the playa deposits (Wadhawan and Kumar, 1996; Cozzi et al., 2012). Its widespread distribution makes it a plausible source of solutes to the groundwater in the Thar Desert. However, the $^{87}Sr/^{86}Sr$ of the playa gypsum (0.71060–0.71238) is considerably more radiogenic than the HEG (c. 0.70866) (Mazumdar and Strauss, 2006), although the mixing of dissolved HEG groundwater with overlying Thar Desert sands (partly

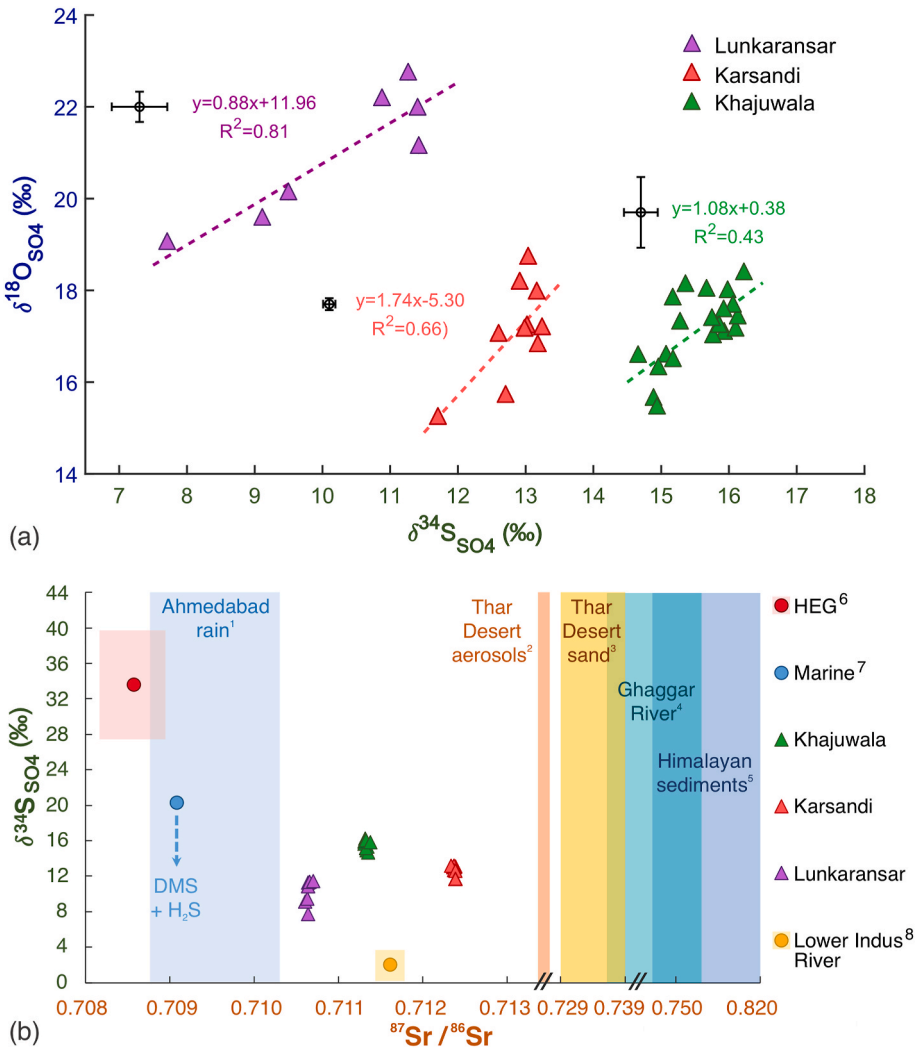

Fig. 7. Top panel (**a**) shows $\delta^{18}O_{SO4}$-$\delta^{34}S_{SO4}$ at Lunkaransar (purple), Karsandi (red), and Khajuwala (green). ± 1σ measurement error bars are shown nearby each of the regression equations. Bottom panel (**b**) shows the $\delta^{34}S$ and $^{87}Sr/^{86}Sr$ ranges of Thar Desert water and sediments, including [1] Ahmedabad rain (Chatterjee and Singh, 2012), [2] Thar Desert aerosols (Yadav and Rajamani, 2004), [3] NE Thar Desert sands (Tripathi et al., 2013), [4] Ghaggar paleochannel sediments (Singh et al., 2016), [5] Himalayan sediments (Krishnaswami and Singh, 1998), [6] Hanseran Evaporite Group deposits (Mazumdar and Strauss, 2006), [7] modern marine water (Rees et al., 1978; Burke et al., 1982), and [8] the modern lower Indus River water (Karim and Veizer, 2000). Double diagonal lines on the x-axis indicate a gap and break in scale. Vertical colored bars are shown for data that only report $^{87}Sr/^{86}Sr$ ranges, and shaded boxes reflect ranges of measured samples. Interaction with dimethylsulfide (DMS) and H_2S decomposition products decreases the $\delta^{34}S$ of marine aerosols, as shown by the dashed blue arrow.

derived from Himalayan sediments) could produce a more radiogenic $^{87}Sr/^{86}Sr$ signature (Fig. 7). However, such a supply of solutes requires a consistent upconing of water from the deep, higher-density, saline aquifers (Lorenzen et al., 2012), which is unlikely on a large spatial and temporal scale.

Similarly, the $\delta^{34}S_{SO4}$ of the investigated playa lakes (7–16 ‰) falls well below that measured for the HEG (27.5–39.7 ‰) (Mazumdar and Strauss, 2006). Lower $\delta^{34}S_{SO4}$ could be attributed to oxidative weathering of pyrite, or atmospheric oxidation of H_2S emissions (Hoefs, 2018). For example, in the Lower Indus River, oxidation of pyrite generates a low $\delta^{34}S_{SO4}$ of c. 2 ‰ in the water (Karim and Veizer, 2000). While the oxidation of pyrite along the groundwater flowpath could lower the $\delta^{34}S_{SO4}$ of sulfate derived from the HEG, the resultant $\delta^{18}O_{SO4}$ would be somewhere between the $\delta^{18}O$ of the water in which the oxidation occurred and 7–12 ‰ higher, depending on how much atmospheric oxygen was present during the oxidation and how much it contributes oxygen atoms to the sulfate (Relph et al., 2021). Given the oxygen isotopic composition of the playa lake paleowater (Fig. 6), it is hard to imagine how the $\delta^{18}O_{SO4}$ could be as high as it is. The fact that the $\delta^{34}S_{SO4}$ and $\delta^{18}O_{SO4}$ are often correlated (Fig. 7) hints that microbial sulfate reduction may have occurred in the fluid from which the sulfate was derived. We note that the slope between the $\delta^{34}S_{SO4}$ and $\delta^{18}O_{SO4}$ is similar to other systems undergoing microbial sulfate reduction (Dogramaci et al., 2001). The nearest notable source of pyrite is the Khetri Copper Belt of the Aravalli mountains, located on the eastern margin of the Thar Desert (Fig. 1), with a $\delta^{34}S$ composition between 5 and 10 ‰ (Jaireth, 1986). Oxidative weathering of pyrite in the Aravalli mountains could be a further potential source of sulfate to the Karsandi playa lake system, which is situated <20 km from a paleochannel linked to the Aravalli mountains. However, such a point source of pyrite would be an unlikely source of sulfur for other playa deposits distributed widely throughout the Thar Desert.

No study has examined the $\delta^{34}S$ of aerosols in the Thar Desert, and the nearest measurements of aerosols in New Delhi are heavily influenced by modern anthropogenic emissions (Sawlani et al., 2019). In the Thar Desert, prevailing southwesterly winds during the Indian Summer Monsoon make a source from marine seasalt aerosols a potential contributor. Modern marine sulfate has a $\delta^{34}S_{SO4}$ of ~20.3 ‰ and a $\delta^{18}O_{SO4}$ of 8.6 ‰ (Rees et al., 1978; Böttcher et al., 2007; Tostevin et al., 2014). As marine-derived seasalt aerosols are formed and travel over the

continent, their sulfur isotope signature can be lowered by oxidation of dimethylsulfide (c. 15 ‰) (Calhoun et al., 1991) or H_2S typically from organic matter in aerosols (Norman et al., 1999; Hoefs, 2018). Whether there would be enough dimethylsulfide or H_2S to impact the overall sulfur isotopic composition isn't clear. The $\delta^{34}S_{SO4}$ from seasalt sulfate would be accompanied by a marine $\delta^{18}O_{SO4}$ signal (8.6 ‰), which could include some amount of sulfate that results from oxidation; this sulfate would typically be higher in its $\delta^{18}O_{SO4}$ because of oxygen isotope equilibration in water vapor that tends to promote equilibration between sulfide and water. We note that if the sole source of sulfate to the Thar Desert playa lakes is seasalt aerosols mixed with sulfate oxidation products along the transport route, then this would not explain the co-variation between the $\delta^{34}S_{SO4}$ and $\delta^{18}O_{SO4}$.

The mixing of rainwater with aerosols derived from the continent influences the $^{87}Sr/^{86}Sr$. Modern marine sulfate has a $^{87}Sr/^{86}Sr$ of 0.70916 (Burke et al., 1982). In Ahmedabad, south of the Thar Desert, rainwater was recorded to have a $^{87}Sr/^{86}Sr$ of 0.70878–0.71027, which was attributed to aerosol mixing of seasalt aerosols with Deccan basalts and Himalayan silicate minerals (Chatterjee and Singh, 2012). Bulk Thar Desert aerosols from Bikaner and Jhunjhunu (cities proximal to the playa lakes) have a more radiogenic $^{87}Sr/^{86}Sr$ of 0.71520–0.71943 (Yadav and Rajamani, 2004), and Thar Desert sand (incorporating fluvial Himalayan sediments) is even more radiogenic at 0.72895–0.73901 (Tripathi et al., 2013). The mixing of rainwater, seasalt aerosols, and Thar Desert sand, along with microbial sulfate reduction in each playa, could therefore produce $\delta^{34}S_{SO4}$, $\delta^{18}O_{SO4}$, and $^{87}Sr/^{86}Sr$ in the range of the playa lakes. Each playa lake would record a distinct signal based on the proportion of different source material in its catchment.

A final consideration involves the remarkably constant value of $^{87}Sr/^{86}Sr$ over thousands of years of deposition (all between 0.71060 and 0.71238, and clustered for each location) (Fig. 7). This lack of variance implies an unchanging mixing ratio between sources, or a single source, and makes an inherently variable source such as groundwater from the HEG less likely. A plausible scenario involves the deposition of marine-derived aerosols in Thar Desert sands over many thousands of years of aridity and dune-building. As moisture increased in the Early Holocene, overland meteoric water run-off into interdunal valleys would dissolve the salts accumulated over this time, preserving a uniform and unique $^{87}Sr/^{86}Sr$ signature for each locality based on a mixture of ancient to modern marine aerosols in a relatively homogeneous matrix of aeolian sediments (Fig. 8). While highly soluble salts like halite would easily dissolve and enter the groundwater, less soluble minerals like gypsum and carbonate would deposit and be preserved in the sedimentary record. An exclusively marine aerosol source of sulfur is not required, and sulfur could also be partially derived from Himalayan fluvial deposits spread throughout the Thar Desert. However, active formation of halite in Lunkaransar playa lake, as well as halite in Didwana, Sambhar, Kanod, Bap-Malar, Pachpadra, Pokhran, and Phulera playa sediments (Roy et al., 2008; Roy and Singhvi, 2016) suggests at least some marine contribution throughout the Thar Desert. The alternative scenario of saline groundwater sourced from the HEG involves less stable mixing pathways because groundwater recharge would continually mix with different volumes of meteoric water. Such mixing also requires a process of oxidation of sulfide minerals in the aquifer to explain the depletion of ^{34}S seen in the playa gypsum.

In conclusion, we suggest that a marine aerosol mixture with Thar Desert sediments and subsequent local modification via microbial sulfate reduction is a plausible scenario for the source of solutes in the majority of playas, due to the stability of $^{87}Sr/^{86}Sr$ and $\delta^{34}S_{SO4}$ throughout thousands of years of gypsum accumulation. This proposal lends support to one of the original models for Thar Desert salt accumulation posited more than 100 years ago (Holland and Christie, 1909). Similarly, the formation of extensive gypsum deposits in the Central

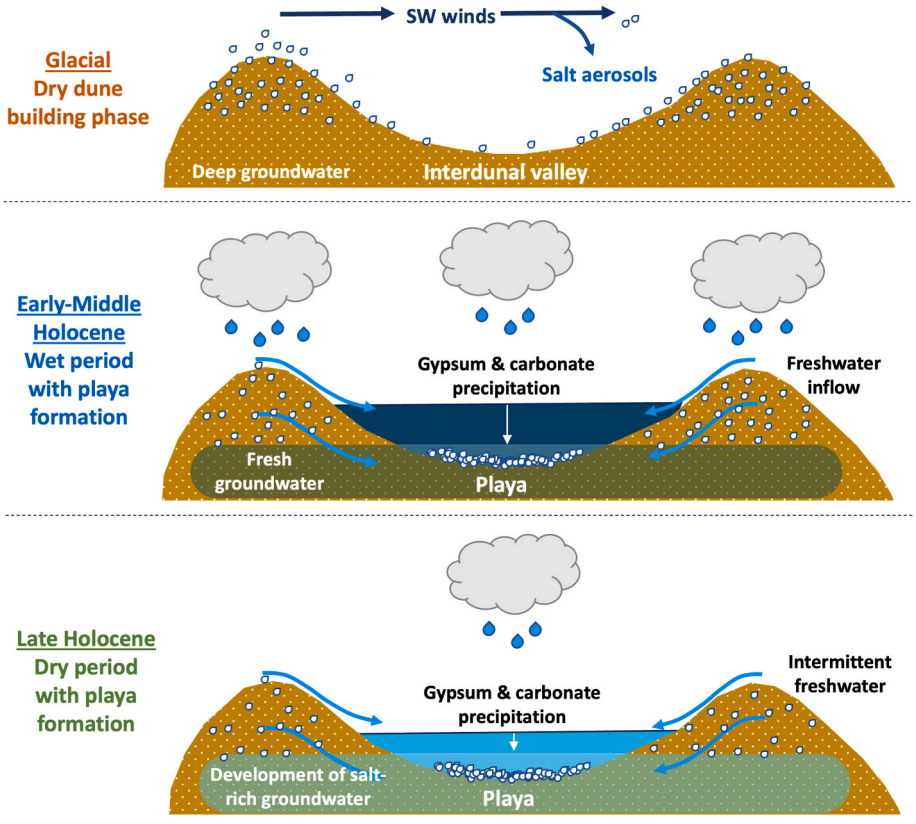

Fig. 8. Conceptual model of solute accumulation during dry dune-building phases and concentration of solutes in playa lakes as gypsum and carbonate deposits during wet and dry periods.

Namib Desert (Eckardt and Spiro, 1999) and the southern and central Australian playas (Chivas et al., 1991), as well as the Atacama desert soil sulfates (Bao et al., 2004; Klipsch et al., 2023), is primarily linked to the deposition of atmospheric sulfate rather than bedrock sulfide sources. In the Australian case, a 55 % contribution of marine "cyclic salts" was estimated for playas up to 1000 km inland (Chivas et al., 1991). Conclusions from these comparable regions lend further credence to the scenario of gypsum formation activated by moisture availability during the Holocene. Theoretically, marine-derived aerosols can contribute salts to the desert during hyper-arid phases with strong winds, and when moisture increases, these sands are a rich source of solutes to form gypsum deposits in depressions such as interdunal valleys (Fig. 8). The solutes dissolve and mix with the local catchment sediments during an influx of rain and groundwater and create a playa-distinct geochemical signature.

4.2. Crystal morphology and implications for playa lake depth

The morphology of gypsum crystals, and what this might reveal about their formation environment, has been studied at great length (e.g., Warren, 1982; Schreiber, 1987; Magee, 1991; Martegani et al., 2024, 2025). While a consensus exists on some diagnostic aspects, other features (e.g., lenticular crystal form) are found in multiple settings, which can complicate their interpretation without additional information (Jafarzadeh and Burnham, 1992; Mees et al., 2012). In the Thar Desert playa lakes from this study, two main forms of gypsum crystals were identified: prismatic and lenticular.

Prismatic crystals (including elongated acicular crystals) are generally found to grow subaqueously on the sediment-water interface of gypsum-saturated brines (Warren, 2006). In contrast, lenticular or lensoidal forms tend to grow in warmer and organic-rich brines (Cody and Cody, 1988), and are often found growing as displacive crystals within surface sediments of seasonally fluctuating regimes (Warren, 1982).

In Lunkaransar, deeper sections of laminated clays containing elongated prismatic gypsum crystals (Supplemental Fig. 7) suggest that they formed in relatively deep water with upward growth, rather than in interstitial sedimentary porewater (Bowler and Teller, 1986). These laminated sediments are similarly interpreted as a lake highstand in previous studies (Singh et al., 1972; Enzel et al., 1999). Clear, prismatic gypsum crystals are also found in the deeper/older section of Khajuwala gypsum deposits (Fig. 9), suggesting a similar stable formation environment with relatively deeper water. The laminations of this unit have classic slump structures that occur due to uneven crystal expansion, which are a defining characteristic of lacustrine gypsum beds identified in the nearby Jamsar gypsum mines (Sundaram and Rakshit, 1994). Prismatic gypsum crystals, which precipitate on the lakebed in sequential order through time and remain preserved, provide the optimal gypsum morphology for making paleoclimatic interpretations based on GHW.

Gypsum disappears at 93–56 cm depth in Lunkaransar, during desiccation of the lakebed, but it re-appears in twinned and lenticular form at the top of the section (Supplemental Fig. 8). Twinned crystals (Supplemental Fig. 8c) are thought to be diagnostic of brines with high concentrations of Ca^{2+}, Na^{+}, SO_4^{2-}, and Cl^{-} (Rodríguez-Aranda et al., 1995), such as those present in Lunkaransar. The lenticular crystal size is generally smaller, which may indicate faster formation at the air-brine interface due to quick supersaturation of a shallow or seasonal regime (Magee, 1991). Such cyclic lake level oscillations tend to form uniform c. 1 mm sized crystals, often as displacive gypsum within the sediment matrix and by evaporation at the capillary fringe of the water table (Magee, 1991). Lenticular gypsum is found throughout most of the Karsandi sequence (Supplemental Fig. 9a), as well as the top 2 m of Khajuwala. In Khajuwala, a distinct zone with tubular encrusted gypsum (Fig. 9b) signifies crystallization around roots or insect burrows during pedogenesis, which indicates yet a further stage of desiccation (cf. Bowler and Teller, 1986).

Finally, the deepest deposits of gypsum at Karsandi have a unique morphology suggesting an initial formation mechanism of this playa in the Early Holocene (Supplemental Fig. 9b). Here, large well-rounded clasts of gypsum (with notably ^{18}O-depleted GHW of −4.78 ‰, markedly lower than the >4 ‰ measured in overlying gypsum) could represent an initial phase of (fluvial) water flowing over gypsiferous sand that produced conglomerate pebbles of gypsum and sand.

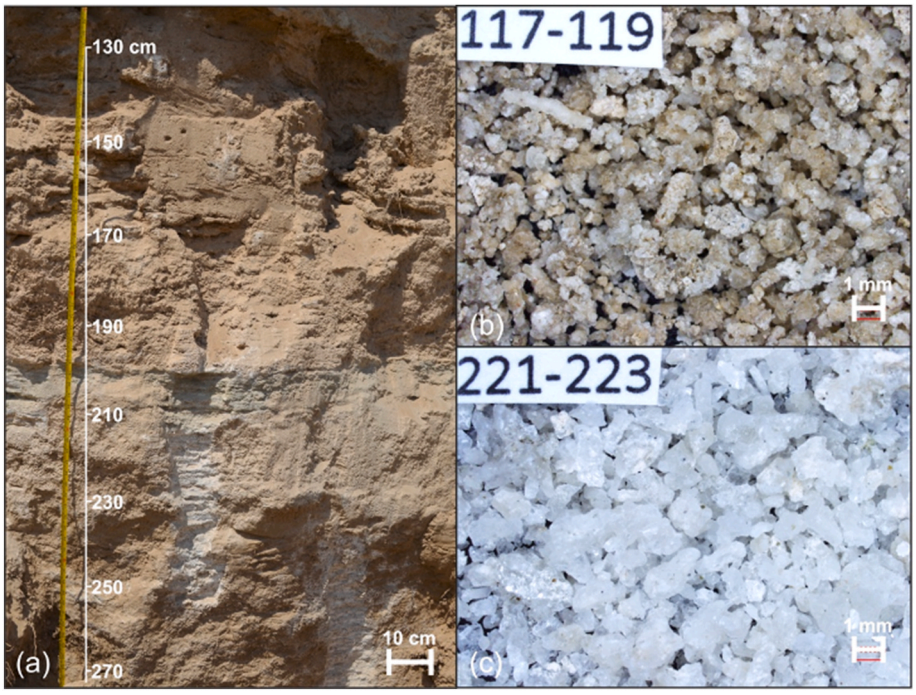

Fig. 9. In Khajuwala, (**a**) section 115–270 cm includes (**b**) gypsum-encrusted tubular structures from a zone of pedogenesis and groundwater infiltration at 117–119 cm depth, in contrast to (**c**) clear, prismatic gypsum crystals from 221 to 223 cm depth.

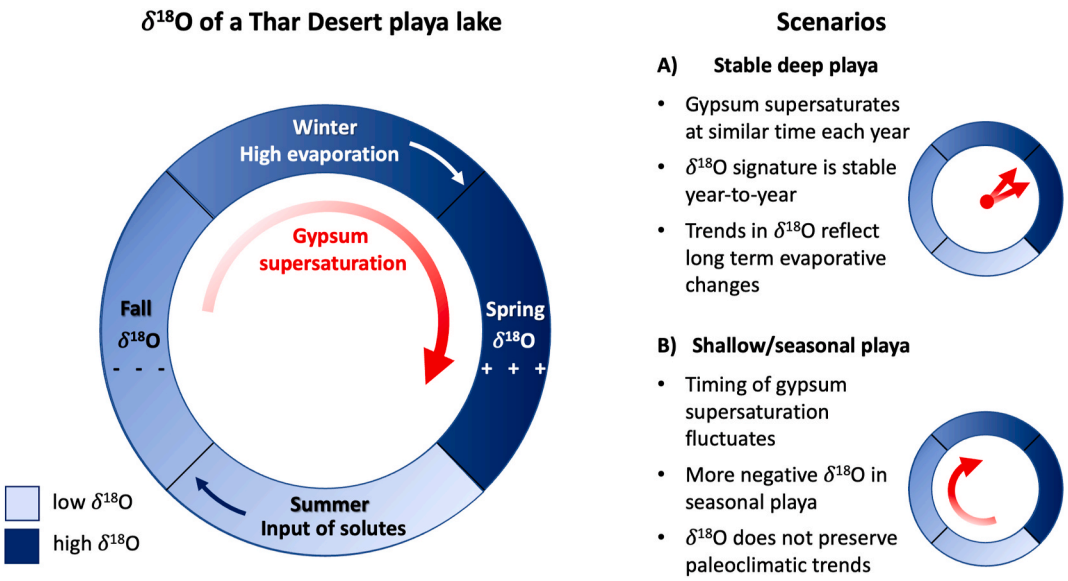

Fig. 10. The seasonal evolution of $\delta^{18}O$ in a playa lake, with solutes and fresh water arriving primarily by summer monsoon rainfall. Evaporation will concentrate the solutes, eventually leading to gypsum supersaturation. The GHW $\delta^{18}O$ will depend on the point at which gypsum supersaturates, which should occur at a similar point of evaporation each year unless the input of solutes is not constant or the playa lake seasonally dries out.

4.3. Seasonal vs. deep playa lakes

Along with the patterns shown by the gypsum crystal morphology (clear prismatic crystals in deep water vs. small sandy lenticular crystals in seasonal pools), we can use the gypsum hydration water isotope values to differentiate environmental conditions. Our samples follow distinct isotopic patterns depending on the depth of playa lake and the likely seasonality of solute saturation (Figs. 6 and 10). This finding agrees with the difference in GHW values measured for gypsum forming in soils vs. playas in the Atacama Desert (Gázquez et al., 2024).

We posit that the GHW isotopic composition of deep playa lakes reflects the isotopic composition of the playa lake water at a fairly consistent time of year when solutes reach supersaturation. In the case of a perennially saturated playa lake in the Thar Desert, the bulk of precipitation (and influx of new solutes) occurs during the Indian Summer Monsoon months during the summer. Following these rainiest months (with minimal additional inputs from the Indian Winter Monsoon months), the lakes trend toward net evaporation during the late winter and spring, concentrating the solutes to the point of supersaturation and gypsum formation (Fig. 10). The timing of supersaturation would remain relatively stable, resulting in GHW isotopic composition that reflects changes in the evaporative balance of the lake (where $\delta^{18}O$ of GHW increases when monsoons are weaker and the lake has experienced more evaporation, and vice versa). The deposition process in deep or perennial playas matches the Early-Middle Holocene scenario depicted in Fig. 8, showing relatively high freshwater inputs to the playa, with gypsum precipitation occurring during periods of high evaporation-to-inflow.

In contrast, the GHW isotopes of seasonal or mostly dry playas are more variable and cannot necessarily be used as a paleohumidity proxy. Here, the supersaturation and deposition of gypsum occurs more unpredictably after rainfall events, which leads to an overall more negative and variable $\delta^{18}O$ (Fig. 10). This matches the Late Holocene scenario in Fig. 8, showing more saline and ephemeral inputs to the playa, where the GHW records a wide range of conditions including very early on in the evaporative process. This aligns with findings that modern GHW isotopes measured across a cross section of a lake in southern Spain reflect progressive drying and evaporation when moving closer to the depocenter of the ephemeral lake (Cañada-Pasadas et al., 2024). While the GHW isotopic composition of lenticular crystals in the upper zones of these playa lakes reflect meteoric and/or groundwater composition at the time of gypsum formation, it may also be difficult to confirm the stratigraphic order of this type of gypsum because of the possibility that solute-rich water infiltrated to variable shallow depths in a seasonally fluctuating playa system (this is unlikely to affect underlying gypsum deposits imbedded in clay). Therefore, we assigned broad age spans to collective units of the playa lake sequences for the following discussion of the GHW paleoclimatic interpretation.

4.4. Paleoclimate inferred by playa lake records

4.4.1. Early Holocene onset of moisture

The start of gypsum deposition and playa lake development in the Thar Desert by itself tells an important story about monsoon intensification after deglaciation, keeping in mind that the age control for all the playa sequences remains imprecise. Deotare et al. (2022) reviewed several Thar Desert playa paleorecords (Sambhar, Didwana, Lunkaransar, Bap-Malar, and Kanod) and concluded that most of these playas were active since at least 15 ka BP and dried by 4 ka BP. The start of playa lake formation is estimated to be post-11.2 ka BP for Karsandi (Dixit et al., 2018), between c. 12.2 and 10.7 ka BP for Khajuwala, and extrapolated to 11.5–9.4 ka BP for Lunkaransar (Singh et al., 1974). Similarly, Kanod and Bap-Malar have layers of silt and aeolian sand followed by laminated silts beginning in the Early Holocene (Deotare et al., 2004), indicating an increase in water depth at that time. Evaporite minerals like halite were accumulating at Didwana since the LGM, but a freshening of the lake was recorded around 13 ka BP (Wasson et al., 1984). Sambhar, on the eastern Thar Desert margin, also has an earlier origin c. 30 ka BP (Sinha et al., 2006), but a transition from sand to clay, marking lake expansion, was dated at just prior to 10.5 ka BP (Singh et al., 1972). The coincidence of these dates point to a regional climatic origin for the increase in moisture throughout the Thar Desert after c. 12 ka BP, possibly aligned with the end of the Younger Dryas (12.9–11.7 ka BP) or the second phase of monsoon intensification proposed around 11.5–10.8 ka BP (Overpeck et al., 1996), as well as a stabilization of dune activity throughout the Thar Desert (Juyal et al., 2003). Increased moisture availability throughout the Thar Desert since 12 ka BP likely drove a desert-wide shift in moisture availability and formation of playa lakes. Local factors including dune activity and river channel movement would also govern the collection of water in these

early playa basins, so further collection of basal dates from other playa sequences in the region would be a valuable contribution towards this analysis.

The average Early to Middle Holocene GHW $\delta^{18}O$ of the three investigated playa lakes was c. 3.9 ‰, and the steeper δD-$\delta^{18}O$ regression slope (Fig. 6 and Supplemental Fig. 5) may indicate that conditions were more humid than during the Late Holocene, assuming the precipitation source water composition was similar. In the bottom meter of Khajuwala's sequence, constrained by two luminescence dates of 12.2 ka BP and 10.7 ka BP, clean prismatic gypsum crystals indicate formation in stable deep playa conditions. During this Early Holocene period, the trend of GHW $\delta^{18}O$ decreases by c. 2.5 ‰ (Fig. 3), suggesting increasingly humid conditions and deepening lake levels in the most arid western part of the Thar Desert. A gradient in relative humidity (drier at Khajuwala in the west, more humid at Karsandi in the northeast) is suggested by the playa-specific clusters of d-excess values in Supplemental Fig. 5. The Middle Holocene part of the gypsum record from Khajuwala appears to be missing due to a hiatus or post-depositional erosion.

Progressing into the Middle Holocene, other playa-based reconstructions in the Thar Desert point to a more humid phase with increased rainfall. For example, pollen reconstructions from Lunkaransar, Sambhar, and Didwana lakes indicate a more humid vegetation landscape with species such as *Artemisia* and *Oldenlandia* that today rarely exist within the arid belt, as well as *Mimosa rubicaulis* in the semi-arid belt, which today mainly grows in regions with >500 mm rainfall (Singh et al., 1974). By c. 5 ka BP, *Syzygium cuminii*, a tropical black plum tree that today grows in areas with >850 mm of annual rainfall, was growing by the easternmost lake at Sambhar, and its distribution appears to have extended as far west as Lunkaransar (Singh et al., 1974). A grassy steppe savannah with scattered trees dominated the landscape during this phase (Singh et al., 1974). Using Lunkaransar's pollen data, a winter and summer rainfall transfer function estimated a c. 200 mm increase in annual rainfall during this period, as well as a doubling of winter precipitation by c. 5 ka BP (Swain et al., 1983). The increase of winter rain (even though only representing a c. 30 mm difference in annual precipitation totals) would have had an especially important effect in decreasing evaporative losses during the dry winter season, thereby resulting in overall higher precipitation efficiency (Bryson and Swain, 1981). The Lunkaransar playa sequence shows laminated clays with prismatic gypsum crystals and GHW $\delta^{18}O$ values decreasing to a relatively low value of 0.9 ‰ (indicating less evaporation) before 6.8 ka BP (Fig. 4). Some of the depths surrounding this gypsum sample contained no gypsum at all, suggesting the lake water did not reach supersaturation needed for gypsum precipitation during this humid phase. The proposed increase in winter rainfall is in good agreement with playa highstands and low GHW $\delta^{18}O$ values at Karsandi between c. 5 and 4.4 ka BP (Fig. 5) (Dixit et al., 2018), as well as a period of higher winter monsoon strength between 4.5 and 4.3 ka BP reconstructed from marine core 63KA by the Indus River delta (Giesche et al., 2019).

4.4.2. Middle to Late Holocene drying

Deotare et al. (2022) concluded that Sambhar, Didwana, Lunkaransar, Bap-Malar, and Kanod playas dried by 4 ka BP. Singhvi and Kar (2004) noted that the western Thar Desert was more quickly destabilized by a lack of rain in the Middle Holocene, with western margin lakes such as Kanod and Bap-Malar drying earlier around 6 ka BP (Deotare et al., 2004), and eastern margin lakes such as Didwana drying by c. 4 ka BP (Singh et al., 1990). Lunkaransar, located midway on the rainfall gradient between Bap Malar and Didwana, shows a transition from laminated clays to oxidized sands that indicates desiccation between 4.7 and 5.5 ka BP (Enzel et al., 1999) or perhaps as late as 4 ka BP (Singh et al., 1974). Sambhar (highest rainfall in the Thar Desert) did not have lowered lake levels until 2.5 ka BP, and even today the lake never completely desiccates (Sinha et al., 2006). Playas in the most arid environments of the western Thar Desert are therefore more sensitive to a retreat in summer monsoon rainfall than eastern playa lakes. Apparently, even a Middle Holocene increase in winter rainfall was not able to compensate for the ongoing retreat in the summer monsoon, producing a sequential drying pattern from west to east. The age control of all lakes is still problematic, and differences in carbon reservoir effects in the dates could explain discrepancies, so this drying pattern requires further testing. Just northeast of the Thar Desert, the drying of Kotla Dahar by 4.1 ka BP appears to be a relatively abrupt event (Dixit et al., 2014). Further north, a Himalayan stalagmite reconstruction shows that both winter and summer rainfall patterns were weakened for several centuries after 4.2 ka BP (Giesche et al., 2023), and a marine core reconstruction from the Arabian Sea suggests a drier regional climate (Giesche et al., 2019), which may correspond to the shallower or in some cases completely desiccated playa lakes in the Thar Desert.

A shift to drier conditions during the Middle to Late Holocene transition is supported by the gypsum hydration records at Lunkaransar (Fig. 4) and Karsandi (Fig. 5). For example, after the radiocarbon date of 6.8 ka BP, Lunkaransar's laminated sediments become increasingly oxidized and have a higher proportion of sand mixed into the gypsum crystals matrix, suggesting shallower lake levels and increased aeolian activity. Simultaneously, GHW $\delta^{18}O$ increases from 1 to 6 ‰, indicating more evaporative conditions during the Middle-Late Holocene transition (**Supplemental Data** and Fig. 4). For some time, gypsum deposition at Lunkaransar completely stops, and does not recommence until sometime after 3.7 ka BP in the Late Holocene, with dirty lenticular crystals in a sandy matrix suggesting an ephemeral or shallow playa lake setting. Karsandi's gypsum deposition also ceases between 4.4 and 3.2 ka BP, replaced by aeolian sand accumulation thereafter (Fig. 5, Dixit et al., 2018).

At Khajuwala, the time period covering 4 ka BP is obscured by a hiatus or post-depositional erosion, though the upper meter of sediments generally indicates a shallow seasonal playa with intermittent presence of water and possible pedogenesis and aeolian accumulation during dry phases. Playa lakes thereby reveal limitations for making any high-resolution paleoclimatic inferences, at least for as long as their chronology remains poorly resolved. However, there is some evidence for a Late Holocene recovery in moisture at Khajuwala that likely spanned at least 1.9–1.3 ka BP, where a phase of gypsum accumulation (shallow or seasonal playa) coincides with the presence of freshwater aquatic gastropods and brackish water ostracods (**Supplemental Materials**). Gypsum deposition also restarts in the top 25 cm of Lunkaransar, with crystal morphology and GHW indicating lower seasonal lake levels and relative humidity compared to the Early-Middle Holocene gypsum (Fig. 4 and Supplemental Fig. 5). This deposition aligns with renewed preservation of pollen at Lunkaransar estimated c. 1.2 ka BP (Singh et al., 1974). However, none of the other playas (including Karsandi) accumulate new gypsum deposits or other sediments formed by water during this time, which points to either a more muted change in climate, or a local factor such as shifts in fluvial pathways or groundwater routes. Aeolian activity was rejuvenated throughout the Thar Desert between 2 and 0.8 ka BP (Singhvi and Kar, 2004), which could have played a role in choking stream pathways and reorganizing water flow along the northern desert margins, as suggested for the Late Holocene (Orengo and Petrie, 2017).

4.4.3. Archaeological implications

The margin of the Thar Desert represents an important climatic ecotone for human subsistence during the Holocene. Indus Civilization sites lie to the north and west of the Thar Desert, and a large number of sites extend into its northern margin (Fig. 11). The region was also inhabited in the Early Historic and Medieval periods. These settlement patterns highlight the importance of playa lake research in the Thar Desert, because the question of water supply (by river, lake, rain, or wells) to such an arid region would have been a primary concern of any settlement (Petrie et al., 2017).

The period of increased moisture from c. 5 to 4.4 ka BP at Karsandi

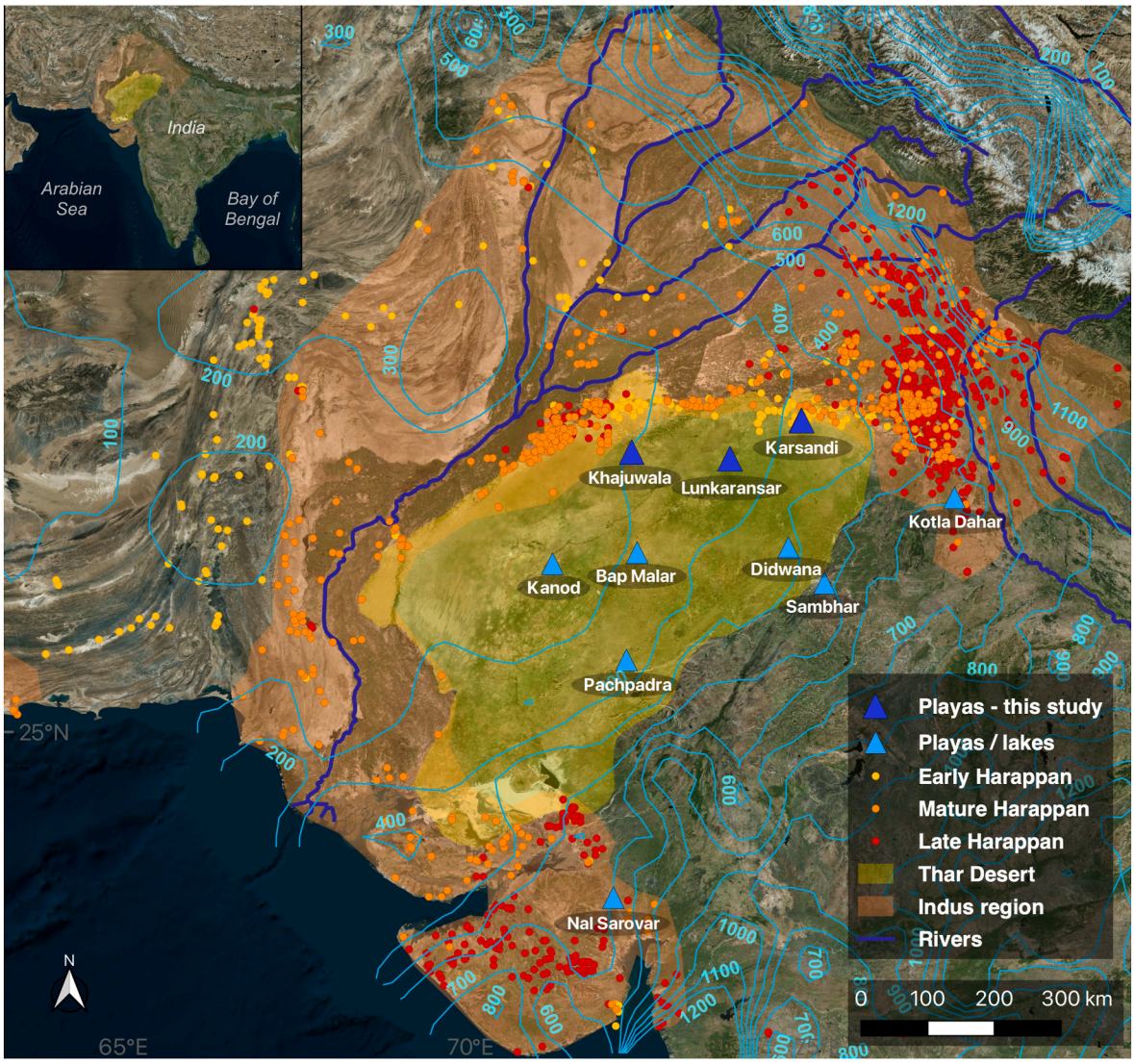

Fig. 11. Thar Desert (yellow shading) playa lakes (blue): Khajuwala, Karsandi (Dixit et al., 2018), Lunkaransar (Singh, 1971; Singh et al., 1972, 1974; Enzel et al., 1999), Sambhar (Singh, 1971; Singh et al., 1972; Sundaram and Pareek, 1995; Sinha et al., 2006), Didwana (Singh, 1971; Singh et al., 1972, 1974, 1990; Wasson et al., 1984), Nal Sarovar (Prasad et al., 1997), Kanod and Bap-Malar (Deotare et al., 1998, 2004), and Pachpadra (Roy et al., 2008). Archaeological sites of the Indus region (orange shading) are shown for the Early Harappan (yellow circles, 5.0–4.6 ka BP), Mature Harappan (orange circles, 4.6–3.9 ka BP), and Late Harappan (red circles, 3.9–3.6 ka BP), with modern mean annual precipitation contours (turquoise) from 0.25° GPCC v2018 1951–2000 rain gauge data (Meyer-Christoffer et al., 2018).

coincides with the appearance of Mature Harappan cities c. 4.6–4.5 ka BP (Dixit et al., 2018). This period may also correspond to the wettest conditions reconstructed by 5 ka BP at Lunkaransar (Singh et al., 1974) linked to increased winter rain (Swain et al., 1983), but is in conflict with another Lunkaransar age model proposing earlier highest lake levels between 7.2 and 5.5 ka BP (Enzel et al., 1999). Overall, during the process of Indus urbanization, it seems likely that the Thar Desert margins were contracted, with relatively higher groundwater levels, increased year-round moisture availability, and lower salinity levels of the playa lakes. The Thar Desert would thus have been an amenable passageway, but, notably, no Indus sites have been identified in the interior desert or its eastern areas (Fig. 11).

The transition to aeolian sediments at Karsandi sometime between 4.4 and 3.2 ka BP broadly overlaps with the onset of urban decline and start of the Late Harappan phase c. 3.9 ka BP (Dixit et al., 2018; also Petrie et al., 2017). This shift would correspond to desiccation dates of 4.0 ka BP at Didwana and Lunkaransar (Singh et al., 1974, 1990), though, again, not with the alternate Lunkaransar date of 5.5 ka BP (Enzel et al., 1999). Our GHW results from Lunkaransar point to progressively more evaporative conditions before eventual desiccation, along with a relatively protracted transition from clay to silt, which would suggest that the transition to aridity was not abrupt here. A gradual decline in moisture would have provided more time for adaptation and migration, as was observed in the transition from more densely populated urban cities to the increase in the number of more resilient rural settlements in the eastern summer-monsoon dominated regions of the Indus region (Possehl, 1997; Petrie et al., 2017; Green and Petrie, 2018; Petrie, 2019).

The possible increase in moisture availability (whether climatic or due to regional fluvial/groundwater factors) during the Late Holocene, noted at Lunkaransar and Khajuwala at c. 1.9–1.3 ka BP, overlaps with a number of historic empires and entities, including the rise of the Kushan and Gupta Empires in India c. 1.9–1.4 ka BP (see Petrie, 2020).

5. Conclusion

This investigation into Thar Desert gypsum has highlighted the wide extent of gypsum as a surficial deposit in Rajasthan, as well as the

tendency for gypsum to accumulate in low-lying interdunal valleys. Although gypsum deposits are generally thought to be a feature of aridity because they require an evaporative environment, they can conversely be regarded as a signal of increased moisture in an arid region with a sufficient supply of solutes. The presence of gypsum in playa lake deposits, in areas that are presently arid or only hold seasonal water, is interpreted as an indicator of enhanced moisture during the Holocene.

Our $\delta^{34}S_{SO4}$ and $^{87}Sr/^{86}Sr$ data from three playa lakes show that marine aerosols should not be discounted as a source of solutes to the Thar Desert. Mixing between meteoric water, accumulated marine-derived aerosols, and Thar Desert sand could explain the stable and playa-distinct $^{87}Sr/^{86}Sr$ signal over thousands of years of gypsum accumulation. Future work, including geochemical measurements of modern aerosols and sand nearby the playas, should be completed in the Thar Desert to explore this theory in more detail, and to estimate the contribution of marine aerosols to the total sulfur content in the Thar Desert. Measuring the ^{17}O and $\delta^{33}S$ of the sulfate component of gypsum could also yield source insights (e.g., Bao et al., 2000; Guibourdenche et al., 2022).

Gypsum accumulation began after c. 12 ka BP at all three investigated sites, indicating increased moisture availability throughout the Thar Desert from a strengthening summer monsoon. At Khajuwala, a progressive decrease in GHW isotope values between c. 12.2–10.7 ka BP shows that conditions became wetter. Gypsum crystal morphology is prismatic at both Khajuwala and Lunkaransar, supporting relatively deeper lake levels with subaqueous gypsum deposition. The Early-Middle Holocene shows comparatively higher relative humidity conditions at Lunkaransar than Khajuwala, and lower than at Karsandi, which reflects the modern relative humidity gradient across the desert.

The dates of Middle-Late Holocene playa lake desiccation suggest a west to east progression of Indian Summer Monsoon retreat in the Thar Desert (Singh et al., 1974, 1990; Enzel et al., 1999; Deotare et al., 2004; Singhvi and Kar, 2004; Sinha et al., 2006), but chronological uncertainties still present a major barrier to confidently interpreting this sequence of events. However, our research suggests that the Middle-Late Holocene transition to aridity at Lunkaransar was relatively gradual, with increasingly evaporative conditions that led to eventual lake desiccation before 3.6 ka BP (minimum age). This may predate or coincide with the drying between 4.4 and 3.2 ka BP reconstructed for Karsandi (Dixit et al., 2018). Culturally, the shift to aridity in the Thar Desert was combined with a shift towards settlements in the Indian Summer Monsoon-dominated northeastern Indus region, which also offers a higher total annual rainfall (Petrie et al., 2017). Compared to the Early-Middle Holocene, the Late Holocene was marked by earlier gypsum supersaturation and lower lake levels at Lunkaransar, along with sandy, lenticular gypsum crystals that reflect shallow or seasonal playa conditions. A potentially coeval episode of lenticular gypsum deposition was interspersed with pedogenesis at Khajuwala between 1.9 and 1.3 ka BP and suggests a short-lived Late Holocene increase in local moisture availability for the northwestern region of the Thar Desert, perhaps through fluvial or groundwater inflow.

Gypsum deposits investigated in this study come from the Bikaner and Hanumangarh districts in India, but substantial deposits in Nagaur, Barmer, Churu, Sri Ganganagar and Jaisalmer districts as well as gypsum from Pakistan should be compared in the future. A particularly deep sequence (>8 m) of lacustrine gypsum from Jamsar playa should be examined, as well as gypsum-rich sediments at Pachpadra playa (Roy et al., 2008), and older Quaternary sequences in Churu and Bikaner that likely contain additional untapped paleoclimatic information (Rakshit and Sundaram, 1998). With the advent of gypsum hydration water analysis as an important paleoclimatic tracer of water isotopes in arid regions (e.g., Hodell et al., 2012; Dixit et al., 2018; Evans et al., 2018), the scientific value of these gypsum deposits has become even more apparent. However, the acceleration of gypsum mining in Rajasthan for cement production today (Bhardwaj, 2016) poses an active threat to the preservation of potential paleoclimatic sequences in the Thar Desert. New mines are being licensed each year, targeting the deepest sections of gypsum. This research points to the importance of preserving archives of gypsum deposits for future geochemical analysis.

Author contributions

A.G., D.A.H., and C.A.P. designed research; A.G., Y.D., V.K.S., R.N.S., and C.A.P. did fieldwork, A.G., F.G., T.B., H.J.B., and R.K.S. performed laboratory research; A.G., A.V.T., H.J.B., F.G., T.B., and D.A.H. analyzed data; A.G. prepared figures and wrote the paper; all authors contributed to editing.

Funding

A.G., D.A.H., and C.A.P. received support from the European Research Council (ERC) under the European Union's Horizon 2020 research and innovation program TwoRains grant agreement no 648609. A.G. and D.A.H. also received support from the European Research Council (ERC) WIHM grant agreement no 339694. F.G. acknowledges the Ramón y Cajal fellowship RYC2020-029811-I and the grant PPIT-UAL Junta de Andalucía-FEDER 2022-2026 (RYC-PPI2021-01).

Declaration of competing interest

The authors declare that they have no known competing financial interests or personal relationships that could have appeared to influence the work reported in this paper.

Acknowledgements

The authors would like to acknowledge several researchers at the University of Cambridge: Dr. Giulio Lampronti for assistance with XRD measurements, Dr. Richard Preece for his assistance with gastropod identification, Dr. Matthew Brady, James Rolfe, and John Nicolson for laboratory assistance with oxygen and hydrogen isotope measurements, and Dr. Emily Stevenson and Dr. Nick Evans for laboratory assistance with strontium measurements. We also thank Dr. Sönke Szidat at the University of Bern and the University of Oxford Radiocarbon Accelerator Unit for AMS measurements. The Border Security Force of India is thanked for granting permission to sample in Rajasthan. We also thank the anonymous reviewers for their careful reading of our manuscript and helpful comments that greatly improved the final version.

Appendix A. Supplementary data

Supplementary data to this article can be found online at https://doi.org/10.1016/j.quascirev.2025.109586.

Data availability

All data and/or code is contained within the submission.

References

Antler, G., Turchyn, A.V., Rennie, V., Herut, B., Sivan, O., 2013. Coupled sulfur and oxygen isotope insight into bacterial sulfate reduction in the natural environment. Geochem. Cosmochim. Acta 118, 98–117. https://doi.org/10.1016/j.gca.2013.05.

Arora, J., Goyal, S., Ramawat, K.G., 2010. Biodiversity, biology and conservation of medicinal plants of the Thar desert. In: Ramawat, K. (Ed.), Desert Plants. Springer, Berlin, Heidelberg, pp. 3–36. https://doi.org/10.1007/978-3-642-02550-1_1.

Baghel, A., Mehta, P., Agrawal, A., 2024. Vernacular architecture of Jodhpur: a resilient approach to sustainable environment. ShodhKosh Journal of Visual and Performing Arts 5 (1), 785–815. https://doi.org/10.29121/shodhkosh.v5.i1.2024.732.

Banerjee, D.M., Rastogi, S.P., Kumar, V., 2012. Some evaporite deposits of India. Proceedings of the Indian National Science Academy 78, 401–406.

Bao, H., Thiemens, M.H., Farquhar, J., Campbell, D.A., Lee, C.C.W., Heine, K., et al., 2000. Anomalous ^{17}O compositions in massive sulphate deposits on the Earth. Nature 406 (6792), 176–178. https://doi.org/10.1038/35018052.

Bao, H., Jenkins, K.A., Khachaturyan, M., Díaz, G.C., 2004. Different sulfate sources and their post-depositional migration in Atacama soils. Earth Planet Sci. Lett. 224 (3–4), 577–587. https://doi.org/10.1016/j.epsl.2004.05.006.

Bauska, T.K., Walters, G., Gázquez, F., Hodell, D.A., 2018. Online differential thermal isotope analysis of hydration water in minerals by cavity Ringdown Laser spectroscopy. Anal. Chem. 90 (1), 752–759. https://doi.org/10.1021/acs.analchem.7b03136.

Bhardwaj, R., 2016. Gypsum: resources of bikaner and new prospective. International Journal of Scientific and Research Publications 6 (2), 68–72. http://www.ijsrp.org/research-paper-0216.php?rp=P505074.

Böttcher, M.E., Brumsack, H.J., Dürselen, C.D., 2007. The isotopic composition of modern seawater sulfate: I. coastal waters with special regard to the North Sea. J. Mar. Syst. 67 (1–2), 73–82. https://doi.org/10.1016/j.jmarsys.2006.09.006.

Bowler, J.M., Teller, J.T., 1986. Quaternary evaporites and hydrological changes, Lake Tyrrell, North-West Victoria. Aust. J. Earth Sci. 33 (1), 43–63. https://doi.org/10.1080/08120098608729349.

Bryson, R.A., Swain, A.M., 1981. Holocene variations of monsoon rainfall in Rajasthan. Quaternary Research 16 (2), 135–145. https://doi.org/10.1016/0033-5894(81)90041-7.

Burke, W.H., Denison, R.E., Hetherington, E.A., Koepnick, R.B., Nelson, H.F., Otto, J.B., 1982. Variation of seawater $^{87}Sr/^{86}Sr$ throughout Phanerozoic time. Geology (10), 516–519. https://doi.org/10.1130/0091-7613(1982)10%3C516:VOSSTP%3E2.0.CO, 2.

Calhoun, J.A., Bates, T.S., Charlson, R.J., 1991. Sulfur isotope measurements of submicrometer sulfate aerosol particles over the Pacific Ocean. Geophys. Res. Lett. 18 (10), 1877–1880. https://doi.org/10.1029/91GL02304.

Cañada-Pasadas, J., Gázquez, F., Martegani, L., Voigt, C., García-Alix, A., Jiménez-Moreno, et al., 2024. Stable isotopes of gypsum hydration water in recent playa-lake sediments: implications for paleoclimate reconstructions. Geogaceta 76, 71–74. https://doi.org/10.55407/geogaceta104479.

Chatterjee, J., Singh, S.K., 2012. $^{87}Sr/^{86}Sr$ and major ion composition of rainwater of Ahmedabad, India: Sources ofsbase cations. Atmos. Environ. 63, 60–67. https://doi.org/10.1016/j.atmosenv.2012.08.060005.

Chawla, S., Dhir, R.P., Singhvi, A.K., 1992. Thermoluminescence chronology of sand profiles in the Thar Desert and their implications. Quat. Sci. Rev. 11 (1–2), 25–32. https://doi.org/10.1016/0277-3791(92)90038-A.

Chivas, A.R., Andrews, A.S., Lyons, W.B., Bird, M.I., Donnelly, T.H., 1991. Isotopic constraints on the origin of salts in Australian playas. 1. Sulphur. Palaeogeogr. Palaeoclimatol. Palaeoecol. 84 (1–4), 309–332. https://doi.org/10.1016/0031-0182(91)90051-R.

Cody, R.D., Cody, A.M., 1988. Gypsum nucleation and crystal morphology in analog saline terrestrial environments. J. Sediment. Res. 58 (2), 247–255. https://doi.org/10.1306/212F8D69-2B24-11D7-8648000102C1865D.

Cozzi, A., Rea, G., Craig, J., 2012. From global geology to hydrocarbon exploration: Ediacaran-Early Cambrian petroleum plays of India, Pakistan and Oman. In: Geological Society, vol. 366. Special Publications, London, pp. 131–162. https://doi.org/10.1144/SP366.14, 1.

Dansgaard, W., 1964. Stable isotopes in precipitation. Tellus 16 (4), 436–468. https://doi.org/10.3402/tellusa.v16i4.8993.

Denison, R.E., Kirkland, D.W., Evans, R., 1998. Using strontium isotopes to determine the age and origin of gypsum and anhydrite beds. J. Geol. 106 (1), 1–18. https://doi.org/10.1086/515996.

Deotare, B.C., Kajale, M.D., Kshirsagar, A.A., Rajaguru, S.N., 1998. Geoarchaeological and palaeoenvironmental studies around Bap-Malar playa, district Jodhpur, Rajasthan. Curr. Sci. 75 (3), 316–320. http://www.jstor.org/stable/24100968.

Deotare, B.C., Kajale, M.D., Rajaguru, S.N., Kusumgar, S., Jull, A.J.T., Donahue, J.D., 2004. Palaeoenvironmental history of Bap-Malar and Kanod playas of western Rajasthan, Thar desert. Proceedings of the Indian Academy of Sciences. Earth and Planetary Sciences 113 (3), 403–425. https://doi.org/10.1007/BF02716734.

Deotare, B.C., Mishra, S., Rajaguru, S.N., 2022. Late Quaternary geoarcheology and palynological studies of some saline lakes of the Thar Desert, Rajasthan, India. In: Kumaran, N., Padmalal, D. (Eds.), Holocene Climate Change and Environment. Elsevier, pp. 547–574.

Dixit, Y., 2013. Holocene Monsoon Variability Inferred from Paleolake Sediments in Northwestern India. Doctoral dissertation, University of Cambridge.

Dixit, Y., Hodell, D.A., Petrie, C.A., 2014. Abrupt weakening of the summer monsoon in northwest India ~4100 yr ago. Geology 42 (4), 339–342. https://doi.org/10.1130/G35236.1.

Dixit, Y., Hodell, D.A., Giesche, A., Tandon, S.K., Gázquez, F., Saini, H.S., et al., 2018. Intensified summer monsoon and the urbanization of Indus Civilization in northwest India. Sci. Rep. 8 (1), 1–8. https://doi.org/10.1038/s41598-018-22504-5.

Dogramaci, S.S., Herczeg, A.L., Schiff, S.L., Bone, Y., 2001. Controls on $\delta^{34}S$ and $\delta^{18}O$ of dissolved sulfate in aquifers of the Murray Basin, Australia and their use as indicators of flow processes. Appl. Geochem. 16 (4), 475–488. https://doi.org/10.1016/S0883-2927(00)00052-4.

Eckardt, F.D., Spiro, B., 1999. The origin of sulphur in gypsum and dissolved sulphate in the Central Namib Desert, Namibia. Sediment. Geol. 123 (3–4), 255–273. https://doi.org/10.1016/S0037-0738(98)00137-7.

Enzel, Y., Sandler, A., Ely, L.L., Mishra, S., Ramesh, R., Amit, R., et al., 1999. High-Resolution Holocene environmental changes in the Thar desert, Northwestern India. Science 284 (5411), 125–128. https://doi.org/10.1126/science.284.5411.125.

Eugster, H.P., 1980. Geochemistry of evaporitic lacustrine deposits. Annu. Rev. Earth Planet Sci. 8 (1), 35–63. https://doi.org/10.1146/annurev.ea.08.050180.000343.

Evans, N.P., Bauska, T.K., Gázquez-Sánchez, F., Brenner, M., Curtis, J.H., Hodell, D.A., 2018. Quantification of drought during the collapse of the classic Maya civilization. Science 361 (6401), 498–501. https://doi.org/10.1126/science.aas9871.

Fröhlich, K., Gibson, J.J., Aggarwal, P.K., 2002. Deuterium Excess in Precipitation and its Climatological Significance. IAEA, pp. 54–66.

Gázquez, F., Hodell, D.A., 2022. Preservation and modification of the isotopic composition ($^{18}O/^{16}O$ and $^{2}H/^{1}H$) of structurally-bound hydration water of gypsum ($CaSO_4 \cdot 2H_2O$) in aqueous solution. Geochem. Cosmochim. Acta 337, 73–81. https://doi.org/10.1016/j.gca.2022.09.042.

Gázquez, F., Mather, I., Rolfe, J., Evans, N.P., Herwartz, D., Staubwasser, M., Hodell, D. A., 2015. Simultaneous analysis of $^{17}O/^{16}O$, $^{18}O/^{16}O$ and $^{2}H/^{1}H$ of gypsum hydration water by cavity ring-down laser spectroscopy. Rapid Commun. Mass Spectrom. 29 (21), 1997–2006. https://doi.org/10.1002/rcm.7312.

Gázquez, F., Evans, N.P., Hodell, D.A., 2017. Precise and accurate isotope fractionation factors ($\alpha^{17}O$, $\alpha^{18}O$ and αD) for water and $CaSO_4 \cdot 2H_2O$ (gypsum). Geochem. Cosmochim. Acta 198, 259–270. https://doi.org/10.1016/j.gca.2016.11.001.

Gázquez, F., Morellón, M., Bauska, T., Herwartz, D., Surma, J., Moreno, A., et al., 2018. Triple oxygen and hydrogen isotopes of gypsum hydration water for quantitative paleo-humidity reconstruction. Earth Planet Sci. Lett. 481, 177–188. https://doi.org/10.1016/j.epsl.2017.10.020.

Gázquez, F., Voigt, C., Claire, M.W., Rull, F., Medina, J., Hodell, D.A., 2024. Revealing the mechanisms of soil gypsum formation in the Atacama Desert through triple oxygen and hydrogen isotopes of gypsum hydration water. Catena 243, 108171. https://doi.org/10.1016/j.catena.2024.108171.

Giesche, A., Staubwasser, M., Petrie, C.A., Hodell, D.A., 2019. Indian winter and summer monsoon strength over the 4.2 ka BP event in foraminifer isotope records from the Indus River delta in the Arabian Sea. Clim. Past 15 (1), 73–90. https://doi.org/10.5194/cp-15-73-2019.

Giesche, A., Hodell, D.A., Petrie, C.A., Haug, G.H., Adkins, J.F., Plessen, B., et al., 2023. Recurring summer and winter droughts from 4.2-3.97 thousand years ago in North India. Commun. Earth Environ. 4 (1), 103. https://doi.org/10.1038/s43247-023-00763-z.

Glennie, K.W., Singhvi, A.K., Lancaster, N., Teller, J.T., 2002. Quaternary climatic changes over Southern Arabia and the Thar Desert, India. In: Geological Society, vol. 195. Special Publications, London, pp. 301–316. https://doi.org/10.1144/GSL.SP.2002.195.01.16, 1.

Godbole, N.N., 1952. The salinity of Sambhar lake. In: Proceedings of Symposium on Rajputana Desert Bull Nat Inst Sci India, vol. 1. National Institute of Sciences of India), New Delhi, India, pp. 89–93.

Goudie, A.S., Sperling, C.H.B., 1977. Long distance transport of foraminiferal tests by wind in the Thar Desert, northwest India. J. Sediment. Res. 47 (2), 630–633. https://doi.org/10.1306/212F71FD-2B24-11D7-8648000102C1865D.

Green, A.S., Petrie, C.A., 2018. Landscapes of urbanization and De-Urbanization: a large-scale approach to investigating the indus civilization's settlement distributions in Northwest India. J. Field Archaeol. 43 (4), 284–299. https://doi.org/10.1080/00934690.2018.1464332.

Guibourdenche, L., Cartigny, P., Pierre, F.D., Natalicchio, M., Aloisi, G., 2022. Cryptic sulfur cycling during the formation of giant gypsum deposits. Earth Planet Sci. Lett. 593, 117676. https://doi.org/10.1016/j.epsl.2022.117676.

Hardie, L.A., Smoot, J.P., Eugster, H.P., 1978. Saline lakes and their deposits: a sedimentological approach. In: Matter, A., Tucker, M.E. (Eds.), Modern and Ancient Lake Sediments. Blackwell Scientific Publications, London, UK, pp. 7–41. https://doi.org/10.1002/9781444303698.ch2.

Hodell, D.A., Turchyn, A.V., Wiseman, C.J., Escobar, J., Curtis, J.H., Brenner, M., et al., 2012. Late Glacial temperature and precipitation changes in the lowland Neotropics by tandem measurement of $\delta^{18}O$ in biogenic carbonate and gypsum hydration water. Geochem. Cosmochim. Acta 77, 352–368. https://doi.org/10.1016/j.gca.2011.11.026.

Hoefs, J., 2018. Stable Isotope Geochemistry, vol. 285. Springer. https://doi.org/10.1007/978-3-030-77692-3.

Holland, T.H., Christie, W.A.K., 1909. The origin of the salt deposits of Rajputana. Record Geol. Surv. India 38 (2), 154–186.

Horibe, Y., Shigehara, K., Takakuwa, Y., 1973. Isotope separation factor of carbon dioxide-water system and isotopic composition of atmospheric oxygen. J. Geophys. Res. 78 (15), 2625–2629. https://doi.org/10.1029/jc078i015p02625.

Jafarzadeh, A.A., Burnham, C.P., 1992. Gypsum crystals in soils. J. Soil Sci. 43 (3), 409–420. https://doi.org/10.1111/j.1365-2389.1992.tb00147.x.

Jaireth, S., 1986. Igneous source of sulfur of sulfides from Madhan-Kudhan and Kolihan deposits, Khetri Copper Belt, Rajasthan. J. Geol. Soc. India 27 (4), 359–368. https://www.geosocindia.org/index.php/jgsi/article/view/65786.

Juyal, N., Kar, A., Rajaguru, S.N., Singhvi, A.K., 2003. Luminescence chronology of aeolian deposition during the Late Quaternary on the southern margin of Thar Desert, India. Quat. Int. 104 (1), 87–98. https://doi.org/10.1016/S1040-6182(02)00137-4.

Kajale, M.D., Deotare, B.C., 1997. Late Quaternary environmental studies on salt lakes in western Rajasthan, India: a summarised view. J. Quat. Sci. 12 (5), 405–412. https://doi.org/10.1002/(SICI)1099-1417(199709/10)12:5<405::AID-JQS323>3.0.CO;2-N.

Karim, A., Veizer, J., 2000. Weathering processes in the Indus River Basin: implications from riverine carbon, sulfur, oxygen, and strontium isotopes. Chem. Geol. 170 (1–4), 153–177. https://doi.org/10.1016/S0009-2541(99)00246-6.

Khademi, H., Mermut, A.R., Krouse, H.R., 1997. Isotopic composition of gypsum hydration water in selected landforms from central Iran. Chem. Geol. 138 (3–4), 245–255. https://doi.org/10.1016/S0009-2541(97)00017-X.

Klipsch, S., Herwartz, D., Voigt, C., Münker, C., Chong, G., Böttcher, et al., 2023. Sulfate sources, biologic cycling, and mobility in Atacama Desert soils revealed by isotope

signatures. Global Planet. Change 230, 104290. https://doi.org/10.1016/j.gloplacha.2023.104290.
Krishnaswami, S., Singh, S.K., 1998. Silicate and carbonate weathering in the drainage basins of the ganga-ghaghara-indus head waters: contributions to major ion and Sr isotope geochemistry. Proc. Indian Acad. Sci. Earth Planet Sci. 107 (4), 283–291. https://doi.org/10.1007/BF02841595.
Liu, T., Artacho, E., Gázquez, F., Walters, G., Hodell, D., 2019. Prediction of equilibrium isotopic fractionation of the gypsum/bassanite/water system using first-principles calculations. Geochem. Cosmochim. Acta 244, 1–11. https://doi.org/10.1016/j.gca.2018.08.045.
Lloyd, R.M., 1968. Oxygen isotope behavior in the sulfate-water System. J. Geophys. Res. 73 (18), 6099–6110. https://doi.org/10.1029/jb073i018p06099.
Lorenzen, G., Sprenger, C., Baudron, P., Gupta, D., Pekdeger, A., 2012. Origin and dynamics of groundwater salinity in the alluvial plains of western Delhi and adjacent territories of Haryana State, India. Hydrol. Process. 26 (15), 2333–2345. https://doi.org/10.1002/hyp.8311.
Luz, B., Barkan, E., 2010. Variations of 17O/16O and 18O/16O in meteoric waters. Geochem. Cosmochim. Acta 74 (22), 6276–6286. https://doi.org/10.1016/j.gca.2010.08.016.
Madella, M., Fuller, D.Q., 2006. Palaeoecology and the Harappan Civilisation of South Asia: a reconsideration. Quat. Sci. Rev. 25 (11–12), 1283–1301. https://doi.org/10.1016/j.quascirev.2005.10.012.
Magee, J.W., 1991. Late quaternary lacustrine, groundwater, aeolian and pedogenic gypsum in the Prungle Lakes, southeastern Australia. Palaeogeogr. Palaeoclimatol. Palaeoecol. 84 (1–4), 3–42. https://doi.org/10.1016/0031-0182(91)90033-N.
Martegani, L., Gázquez, F., Voigt, C., Jiménez Bonilla, A., Rodríguez Rodríguez, M., Reicherter, K., 2024. Gypsum crystal morphologies in lake sediments for paleoclimate reconstructions: a case study in Fuente de Piedra playa-lake (Málaga). Geogaceta 76, 11–14. https://doi.org/10.55407/geogaceta104492.
Martegani, L., Gázquez, F., Voigt, C., Jiménez-Bonilla, A., Rodríguez-Rodríguez, M., Reicherter, K., 2025. Late Pleistocene-Holocene lake-groundwater interaction in Fuente de Piedra playa-lake (southern Iberian Peninsula) recorded by stable isotopes of gypsum hydration water. Catena 254, 108949. https://doi.org/10.1016/j.catena.2025.108949.
Mathur, L.N., 2008. Geoscientific studies and managing Lakes of arid and semi-arid regions of Rajasthan. In: Sengupta, M., Dalwani, R. (Eds.), Proceedings of Taal 2007: the 12th World Lake Conference. Indian Ministry of Environment and Forest), Jaipur, India, pp. 1928–1932.
Mazumdar, A., Strauss, H., 2006. Sulfur and strontium isotopic compositions of carbonate and evaporite rocks from the late Neoproterozoic-early Cambrian Bilara Group (Nagaur-Ganganagar Basin, India): constraints on intrabasinal correlation and global sulfur cycle. Precambr. Res. 149 (3–4), 217–230. https://doi.org/10.1016/j.precamres.2006.06.008.
Mees, F., Casteneda, C., Herrero, J., Van Ranst, E., 2012. The Nature and significance of variations in Gypsum crystal morphology in dry Lake basins. J. Sediment. Res. 82 (1), 37–52. https://doi.org/10.2110/jsr.2012.3.
Meyer-Christoffer, A., Becker, A., Finger, P., Schneider, U., Ziese, M., 2018. GPCC climatology version 2018 at 0.25°: monthly land-surface precipitation climatology for every month and the total year from rain-gauges built on GTS-based and historical data. https://doi.org/10.5676/DWD_GPCC/CLIM_M_V2018_025.
Midhuna, T.M., Kumar, P., Dimri, A.P., 2020. A new Western Disturbance Index for the Indian winter monsoon. J. Earth Syst. Sci. 129 (1). https://doi.org/10.1007/s12040-019-1324-1.
Norman, A.L., Barrie, L.A., Toom-Sauntry, D., Sirois, A., Krouse, H.R., Li, S.M., et al., 1999. Sources of aerosol sulphate at alert: Apportionment using stable isotopes. Journal of Geophysical Research Atmospheres 104 (D9), 11619–11631. https://doi.org/10.1029/1999JD900078.
Orengo, H.A., Petrie, C.A., 2017. Large-scale, multi-temporal remote sensing of palaeo-river networks: a case study from Northwest India and its implications for the Indus Civilisation. Remote Sens. 9 (7), 1–20. https://doi.org/10.3390/rs9070735.
Overpeck, J., Anderson, D., Trumbore, S., Prell, W., 1996. The southwest Indian Monsoon over the last 18000 years. Clim. Dyn. 12 (3), 213–225. https://doi.org/10.1007/BF00211619.
Pang, H., He, Y., Zhang, Z., Lu, A., Gu, J., 2004. The origin of summer monsoon rainfall at New Delhi by deuterium excess. Hydrol. Earth Syst. Sci. 8 (1), 115–118. https://doi.org/10.5194/hess-8-115-2004.
Petrie, C.A., Singh, R.N., Bates, J., Dixit, Y., French, C.A.I., Hodell, D.A., et al., 2017. Adaptation to variable environments, resilience to climate change: investigating land, water and settlement in Indus Northwest India. Curr. Anthropol. 58 (1), 1–30. https://doi.org/10.1086/690112.
Petrie, C.A., 2019. Diversity, variability, adaptation and 'fragility' in the Indus Civilization. In: Yoffee, N. (Ed.), The Evolution of Fragility: Settling the Terms. McDonald Institute for Archaeological Research, Cambridge, UK, pp. 109–133. https://doi.org/10.17863/CAM.40701.
Petrie, C.A., 2020. Resistance at the Edge of Empires: the Archaeology and History of the Bannu Basin from 1000 BC to AD 1200. Oxbow Books, Oxford, UK. https://doi.org/10.2307/j.ctv13pk77m.
Possehl, G.L., 1997. Climate and the eclipse of the ancient cities of the indus. In: Dalfes, H.N., Kukla, G., Weiss, H. (Eds.), Third Millennium BC Climate Change and Old World Collapse. Springer, Berlin, Germany, pp. 193–243. https://doi.org/10.1007/978-3-642-60616-8_8.
Prasad, S., Kusumgar, S., Gupta, S.K., 1997. A mid to late Holocene record of palaeoclimatic changes from Nal Sarovar: a palaeodesert margin lake in western India. J. Quat. Sci. 12 (2), 153–159. https://doi.org/10.1002/(SICI)1099-1417(199703/04)12:2<153::AID-JQS300>3.0.CO;2-X.
Prasad, S., Enzel, Y., 2006. Holocene paleoclimates of India. Quaternary Research 66 (3), 442–453. https://doi.org/10.1016/j.yqres.2006.05.008.
Rakshit, P., Sundaram, R.M., 1998. Calcrete and gypsum crusts of the Thar Desert, Rajasthan, their geomorphic locales and use as palaeoclimatic indicators. J. Geol. Soc. India 51 (2), 249–255. https://doi.org/10.17491/jgsi/1998/510215.
Ramesh, R., Jani, R.A., Bhushan, R., 1993. Stable isotopic evidence for the origin of salt lakes in the Thar desert. J. Arid Environ. 25 (1), 117–123. https://doi.org/10.1006/jare.1993.1047.
Rees, C.E., Jenkins, W.J., Monster, J., 1978. The sulphur isotopic composition of ocean water sulphate. Geochem. Cosmochim. Acta 42 (4), 377–381. https://doi.org/10.1016/0016-7037(78)90268-5.
Relph, K.E., Stevenson, E.I., Turchyn, A.V., Antler, G., Bickle, M.J., Baronas, J.J., et al., 2021. Partitioning riverine sulfate sources using oxygen and sulfur isotopes: implications for carbon budgets of large rivers. Earth Planet Sci. Lett. 567, 116957. https://doi.org/10.1016/j.epsl.2021.116957.
Rodríguez-Aranda, J.P., Rouchy, J.M., Calvo, J.P., Ordóñez, S., del Cura, M.A.G., 1995. Unusual twinning features in large primary gypsum crystals formed in salt lake conditions, middle Miocene, Madrid Basin, Spain—Palaeoenvironmental implications. Sediment. Geol. 95 (1–2), 123–132. https://doi.org/10.1016/0037-0738(95)00107-7.
Rosen, M.R., 1994. The importance of groundwater in playas: a review of playa classifications and the sedimentology and hydrology of playas. In: Rosen, M.R. (Ed.), Paleoclimate and Basin Evolution of Playa Systems. Geological Society of America, Boulder, CO, USA, pp. 1–18. https://doi.org/10.1130/SPE289-p1.
Roy, A.B., 1999. Evolution of saline lakes in Rajasthan. Curr. Sci. 76 (3), 290–295. https://www.jstor.org/stable/24101124.
Roy, P.D., Smykatz-Kloss, W., 2007. REE geochemistry of the recent playa sediments from the Thar Desert, India: an implication to playa sediment provenance. Geochemistry 67 (1), 55–68. https://doi.org/10.1016/j.chemer.2005.01.006.
Roy, P.D., Smykatz-Kloss, W., Morton, O., 2008. Geochemical zones and reconstruction of late Holocene environments from shallow core sediments of the Pachapadra paleo-lake, Thar Desert, India. Chem. Erde 68 (3), 313–322. https://doi.org/10.1016/j.chemer.2006.01.006.
Roy, P.D., Singhvi, A.K., 2016. Climate variation in the Thar desert since the last glacial maximum and evaluation of the Indian monsoon. TIP 19 (1), 32–44. https://doi.org/10.1016/j.recqb.2016.02.004.
Saini, H.S., Tandon, S.K., Mujtaba, S.A.I., Pant, N.C., 2005. Lake deposits of the northeastern margin of Thar Desert: holocene(?) palaeoclimatic implications. Curr. Sci. 88 (12), 1994–2000.
Sawlani, R., Agnihotri, R., Sharma, C., Patra, P.K., Dimri, A.P., Ram, K., et al., 2019. The severe Delhi SMOG of 2016: a case of delayed crop residue burning, coincident firecracker emissions, and atypical meteorology. Atmos. Pollut. Res. 10 (3), 868–879. https://doi.org/10.1016/j.apr.2018.12.015.
Schreiber, B.C., 1987. Environments of subaqueous gypsum deposition. In: Dean, W.E., Schreiber, B.C. (Eds.), Marine Evaporites S.E.P.M. Short Course 4. SEPM Society of Sedimentary Geology), Oklahoma City, OK, pp. 43–73. https://doi.org/10.2110/scn.78.01.0043.
Schreiber, B., El Tabakh, M., 2000. Deposition and early alteration of evaporites. Sedimentology 47, 215–238. https://doi.org/10.1046/j.1365-3091.2000.00002.x.
Shrivastava, P., Gupta, P., Malhotra, G., 2011. Geology and mineral resources of Rajasthan. Report. Geological Survey of India 30, 1–130.
Singh, A., Paul, D., Sinha, R., Thomsen, K.J., Gupta, S., 2016. Geochemistry of buried river sediments from Ghaggar Plains, NW India: Multi-proxy records of variations in provenance, paleoclimate, and paleovegetation patterns in the Late Quaternary. Palaeogeogr. Palaeoclimatol. Palaeoecol. 449, 85–100. https://doi.org/10.1016/j.palaeo.2016.02.012.
Singh, G., 1971. The Indus Valley culture: seen in the context of post-glacial climatic and ecological studies in north-west India. Archaeol. Phys. Anthropol. Ocean. 6 (2), 177–189. https://doi.org/10.1002/j.1834-4453.1971.tb00134.x.
Singh, G., Joshi, R.D., Singh, A.B., 1972. Stratigraphic and radiocarbon evidence for the age and development of three salt lake deposits in Rajasthan, India. Quaternary Research 2 (4), 496–505. https://doi.org/10.1016/0033-5894(72)90088-9.
Singh, G., Joshi, R.D., Chopra, S.K., Singh, A.B., 1974. Late Quaternary history of vegetation and climate of the Rajasthan Desert, India. Philosophical Transactions of the Royal Society of London Biological Sciences 267 (889), 467–501. https://doi.org/10.1098/rstb.1974.0006.
Singh, G., Wasson, R.J., Agrawal, D.P., 1990. Vegetational and seasonal climatic changes since the last full glacial in the Thar Desert, northwestern India. Rev. Palaeobot. Palynol. 64 (1–4), 351–358. https://doi.org/10.1016/0034-6667(90)90151-8.
Singhvi, A.K., Kar, A., 2004. The aeolian sedimentation record of the Thar desert. Proc. Indian Acad. Sci. Earth Planet Sci. 113 (3), 371–401. https://doi.org/10.1007/BF02716733.
Singhvi, A.K., Williams, M.A.J., Rajaguru, S.N., Misra, V.N., Chawla, S., Stokes, S., et al., 2010. A ~200 ka record of climatic change and dune activity in the Thar Desert, India. Quat. Sci. Rev. 29 (23–24), 3095–3105. https://doi.org/10.1016/j.quascirev.2010.08.003.
Sinha, R., Smykatz-Kloss, W., Stüben, D., Harrison, S.P., Berner, Z., Kramar, U., 2006. Late Quaternary palaeoclimatic reconstruction from the lacustrine sediments of the Sambhar playa core, Thar Desert margin, India. Palaeogeogr. Palaeoclimatol. Palaeoecol. 233 (3–4), 252–270. https://doi.org/10.1016/j.palaeo.2005.09.012.
Sofer, Z., 1978. Isotopic composition of hydration water in gypsum. Geochem. Cosmochim. Acta 42 (8), 1141–1149. https://doi.org/10.1016/0016-7037(78)90109-6.
Srivastava, A., Thomas, D.S., Durcan, J.A., 2019. Holocene dune activity in the Thar Desert, India. Earth Surf. Process. Landf. 44 (7), 1407–1418. https://doi.org/10.1002/esp.4583.

Sun, T., Bao, H., Reich, M., Hemming, S.R., 2018. More than ten million years of hyperaridity recorded in the Atacama Gravels. Geochem. Cosmochim. Acta 227, 123–132. https://doi.org/10.1016/j.gca.2018.02.021.

Sundaram, R.M., Rakshit, P., 1994. Occurrence and origin of gypsum deposits at Jamsar and Pallu in northwest Rajasthan. Ann. Arid Zone 33, 105–108.

Sundaram, R.M., Pareek, S., 1995. Quaternary Facies and paleoenvironment in north and East of sambhar Lake, Rajasthan. J. Geol. Soc. India 46 (4), 385–392. https://doi.org/10.17491/jgsi/1995/460409.

Swain, A.M., Kutzbach, J.E., Hastenrath, S., 1983. Estimates of Holocene precipitation for Rajasthan, India, based on pollen and lake-level data. Quaternary Research 19 (1), 1–17. https://doi.org/10.1016/0033-5894(83)90024-8.

Thomas, J.V., Kar, A., Kailath, A.J., Juyal, N., Rajaguru, S.N., 1999. Late Pleistocene-Holocene history of aeolian accumulation in the Thar Desert, India. Zeitschrift Für Geomorphologie. Supplementband 116, 181–194.

Tostevin, R., Turchyn, A.V., Farquhar, J., Johnston, D.T., Eldridge, D.L., Bishop, J.K., et al., 2014. Multiple sulfur isotope constraints on the modern sulfur cycle. Earth Planet Sci. Lett. 396, 14–21. https://doi.org/10.1016/j.epsl.2014.03.057.

Tripathi, J.K., Bock, B., Rajamani, V., 2013. Nd and Sr isotope characteristics of Quaternary Indo-Gangetic Plain sediments: source distinctiveness in different geographic regions and its geological significance. Chem. Geol. 344, 12–22. https://doi.org/10.1016/j.chemgeo.2013.02.016.

Usman, M., Clift, P.D., Pastore, G., Vezzoli, G., Andò, S., Barbarano, M., et al., 2024. Climatic influence on sediment distribution and transport in the Thar Desert (Sindh and Cholistan, Pakistan). Earth Sci. Rev. 249, 104674. https://doi.org/10.1016/j.earscirev.2024.104674.

Wadhawan, S.K., Kumar, V., 1996. Subsurface Quaternary aeolian stratigraphy in the Ghaggar basin of Thar Desert, India. J. Arid Environ. 32 (1), 37–51. https://doi.org/10.1006/jare.1996.0004.

Warren, J.K., 1982. The hydrological setting, occurrence and significance of gypsum in late Quaternary salt lakes in South Australia. Sedimentology 29 (5), 609–637. https://doi.org/10.1111/j.1365-3091.1982.tb00071.x.

Warren, J.K., 2006. Evaporites: Sediments, Resources and Hydrocarbons. Springer, Berlin. https://doi.org/10.1007/3-540-32344-9.

Wasson, R.J., Rajaguru, S.N., Misra, V.N., Agrawal, D.P., Dhir, R.P., Singhvi, A.K., et al., 1983. Geomorphology, late Quaternary stratigraphy and paleoclimatology of the Thar dunefield. Zeitschrift Für Geomorphologie. Supplementband 45, 117–151.

Wasson, R.J., Smith, G.I., Agrawal, D.P., 1984. Late quaternary sediments, minerals, and inferred geochemical history of Didwana Lake, Thar Desert, India. Palaeogeogr. Palaeoclimatol. Palaeoecol. 46 (4), 345–372. https://doi.org/10.1016/0031-0182(84)90006-3.

Yadav, S., Rajamani, V., 2004. Geochemistry of aerosols of northwestern part of India adjoining the Thar desert. Geochem. Cosmochim. Acta 68 (9), 1975–1988. https://doi.org/10.1016/j.gca.2003.10.032.

Yadav, D.N., Sarin, M.M., 2009. Geo-chemical behavior of uranium in the Sambhar salt lake, Rajasthan (India): implications to “Source” of salt and uranium “Sink.”. Aquat. Geochem. 15 (4), 529–545. https://doi.org/10.1021/jf4051599.